

Selective regulation of IP₃-receptor-mediated Ca²⁺ signaling and apoptosis by the BH4 domain of Bcl-2 versus Bcl-XI

G Monaco^{1,5}, E Decrock^{2,5}, H Akl¹, R Ponsaerts¹, T Vervliet¹, T Luyten¹, M De Maeyer³, L Missiaen¹, CW Distelhorst⁴, H De Smedt¹, JB Parys¹, L Leybaert² and G Bultynck^{*1}

Antiapoptotic B-cell lymphoma 2 (Bcl-2) targets the inositol 1,4,5-trisphosphate receptor (IP₃R) via its BH4 domain, thereby suppressing IP₃R Ca²⁺-flux properties and protecting against Ca²⁺-dependent apoptosis. Here, we directly compared IP₃R inhibition by BH4-Bcl-2 and BH4-Bcl-XI. In contrast to BH4-Bcl-2, BH4-Bcl-XI neither bound the modulatory domain of IP₃R nor inhibited IP₃-induced Ca²⁺ release (IICR) in permeabilized and intact cells. We identified a critical residue in BH4-Bcl-2 (Lys17) not conserved in BH4-Bcl-XI (Asp11). Changing Lys17 into Asp in BH4-Bcl-2 completely abolished its IP₃R-binding and -inhibitory properties, whereas changing Asp11 into Lys in BH4-Bcl-XI induced IP₃R binding and inhibition. This difference in IP₃R regulation between BH4-Bcl-2 and BH4-Bcl-XI controls their antiapoptotic action. Although both BH4-Bcl-2 and BH4-Bcl-XI had antiapoptotic activity, BH4-Bcl-2 was more potent than BH4-Bcl-XI. The effect of BH4-Bcl-2, but not of BH4-Bcl-XI, depended on its binding to IP₃Rs. In agreement with the IP₃R-binding properties, the antiapoptotic activity of BH4-Bcl-2 and BH4-Bcl-XI was modulated by the Lys/Asp substitutions. Changing Lys17 into Asp in full-length Bcl-2 significantly decreased its binding to the IP₃R, its ability to inhibit IICR and its protection against apoptotic stimuli. A single amino-acid difference between BH4-Bcl-2 and BH4-Bcl-XI therefore underlies differential regulation of IP₃Rs and Ca²⁺-driven apoptosis by these functional domains. Mutating this residue affects the function of Bcl-2 in Ca²⁺ signaling and apoptosis.

Cell Death and Differentiation (2012) 19, 295–309; doi:10.1038/cdd.2011.97; published online 5 August 2011

Pro- and anti-apoptotic B-cell lymphoma 2 (Bcl-2) family members control cell survival by regulating programmed cell death and autophagy.¹ The founding member is Bcl-2, a 26-kDa protein localized in the mitochondrial and endoplasmic-reticulum (ER) membranes. Members of this protein family are characterized by the presence of Bcl-2 homology domains (BH domains).^{2,3} Although multidomain proapoptotic proteins contain three BH domains (BH1, BH2 and BH3), the antiapoptotic proteins, like Bcl-2 and Bcl-XI, are characterized by an additional BH domain (BH4).¹ The BH1, BH3 and BH2 domains of the antiapoptotic Bcl-2 family proteins form a hydrophobic pocket that binds the BH3 domain of proapoptotic proteins, thereby counteracting their proapoptotic activity.⁴ Besides this hydrophobic cleft,

the BH4 domain is also essential for the antiapoptotic activity of Bcl-2.^{5,6}

Moreover, Ca²⁺ signaling from the ER to the mitochondria plays an important role in apoptosis initiation.⁷ Several pro- and anti-apoptotic Bcl-2 proteins localize at the ER membrane, where they modulate Ca²⁺-release events^{8,9} (recently reviewed in Rong *et al.*¹⁰ and Rizzuto *et al.*¹¹). Bcl-2 proteins thereby influence mitochondrial function because of the close proximity of ER and mitochondrial membranes.^{12–14} Ca²⁺ transfer via the ER–mitochondria connection plays a bimodal role in cell survival.^{15,16} Small oscillatory Ca²⁺ signals promote survival by stimulating mitochondrial function and bioenergetics, whereas larger mitochondrial [Ca²⁺] rises promote cell death by provoking mitochondrial outer

¹Laboratory of Molecular and Cellular Signaling, Department of Molecular Cell Biology, Campus Gasthuisberg O/N-1 bus 802, Herestraat 49, BE-3000 Leuven, Belgium;

²Department of Basic Medical Sciences, Physiology Group, Faculty of Medicine and Health Sciences, Ghent University, BE-9000 Ghent, Belgium; ³Biomolecular Modelling, Biochemistry, Molecular and Structural Biology Section, Department of Chemistry, Celestijnenlaan 200G bus 2403, BE-3001 Heverlee, Belgium and

⁴Departments of Medicine and Pharmacology, Comprehensive Cancer Center, Case Western Reserve University, Cleveland, OH 44106, USA

*Corresponding author: G Bultynck, Laboratory of Molecular and Cellular Signaling, Department Molecular Cell Biology, Campus Gasthuisberg O/N-1 bus 802, Herestraat 49, BE-3000 Leuven, Belgium. Tel: +32 16 330215; Fax: +32 16 345991; E-mail: geert.bultynck@med.kuleuven.be

⁵These authors contributed equally to this work.

Keywords: apoptosis; antiapoptotic Bcl-2-family members; calcium signaling; endoplasmic reticulum; intracellular Ca²⁺-release channels

Abbreviations: AI, apoptotic index; ATP, adenosine 5'-triphosphate; AUC, area under the curve; Bcl, B-cell lymphoma; BH domain, Bcl-2 homology domain; BSA, bovine serum albumin; Caspase, cysteine-dependent aspartate-specific protease; CED, cell death abnormal; c.p.m., counts per min; CytC, cytochrome c; DTR, Dextran Texas Red; EGTA, ethylene glycol tetraacetic acid; ER, endoplasmic reticulum; FACS, fluorescence-activated cell sorting; FITC, fluorescein isothiocyanate; GST, glutathione-S-transferase; HBSS, Hanks' balanced salt solution; HRP, horseradish peroxidase; IC, inhibitory concentration; IDP, IP₃R-derived peptide; IICR, IP₃-induced Ca²⁺ release; IP₃, inositol 1,4,5-trisphosphate; IP₃R, inositol 1,4,5-trisphosphate receptor; K_d, dissociation constant; MEF, mouse embryonic fibroblast; MOMP, mitochondrial outer membrane permeabilization; NFAT, nuclear factor of activated T cells; NF-κB, nuclear factor kappa-light-chain enhancer of activated B cells; PAC-1, first procaspase activating compound; PAGE, polyacrylamide gel electrophoresis; PARP, poly-(ADP-ribose)-polymerase; PBS, phosphate-buffered saline; PFA, paraformaldehyde; PI, propidium iodide; PVDF, polyvinylidene fluoride; RAF-1, v-raf-1 murine leukemia viral oncogene homolog 1; RAS, RA1 Sarcoma; RU, resonance/response unit; SDS, sodium dodecyl sulfate; SPR, surface plasmon resonance; SERCA, sarcoplasmic-endoplasmic-reticulum Ca²⁺ adenosine triphosphatase; STS, staurosporine; TG, thapsigargin; VDAC, voltage-dependent anion channel

Received 02.12.10; revised 02.5.11; accepted 13.6.11; Edited by L Scorrano; published online 05.8.11

membrane permeabilization (MOMP).^{11,13,14,17,18} Thus, both promoting cytosolic Ca^{2+} oscillations and blunting cytosolic Ca^{2+} transients underpin the antiapoptotic action of Bcl-2 family members.¹⁹

Different studies demonstrated that inositol 1,4,5-trisphosphate receptors (IP_3Rs) play a central role in this paradigm as targets of Bcl-2, Bcl-XI and Mcl-1.^{20–25} However, the localization of their interaction sites on the IP_3R as well as the physiological roles of these interactions remain unsolved. Different, not mutually exclusive, mechanisms have been proposed. (1) Increasing the ratio of anti- over pro-apoptotic Bcl-2 proteins caused IP_3R sensitization, enhancing basal IP_3R -mediated Ca^{2+} leak and reducing steady-state $[\text{Ca}^{2+}]$ in the ER.²⁰ (2) Bcl-XI interacted with the C-terminus of IP_3Rs , promoting spontaneous Ca^{2+} oscillations and enhancing mitochondrial bioenergetics.^{23,26} (3) Bcl-2 directly inhibited IP_3Rs without altering steady-state ER Ca^{2+} levels.^{21,22,27} Recently, the Bcl-2 interaction domain was identified in the central, modulatory region of the IP_3R (amino acids (a.a.) 1389–1408).²⁸ Disturbing endogenous IP_3R /Bcl-2 complexes potentiated IP_3 -induced Ca^{2+} release (IICR) and sensitized cells toward proapoptotic Ca^{2+} signaling.²⁸ The BH4 domain of Bcl-2 was necessary and sufficient for interaction with the IP_3R .^{29,30} (4) Bcl-XI reduced the expression levels of IP_3Rs via a decreased binding of NFATc2 (nuclear factor of activated T cells, cytoplasmic, calcineurin-dependent 2) to the IP_3R promoter,³¹ thereby reducing IICR.

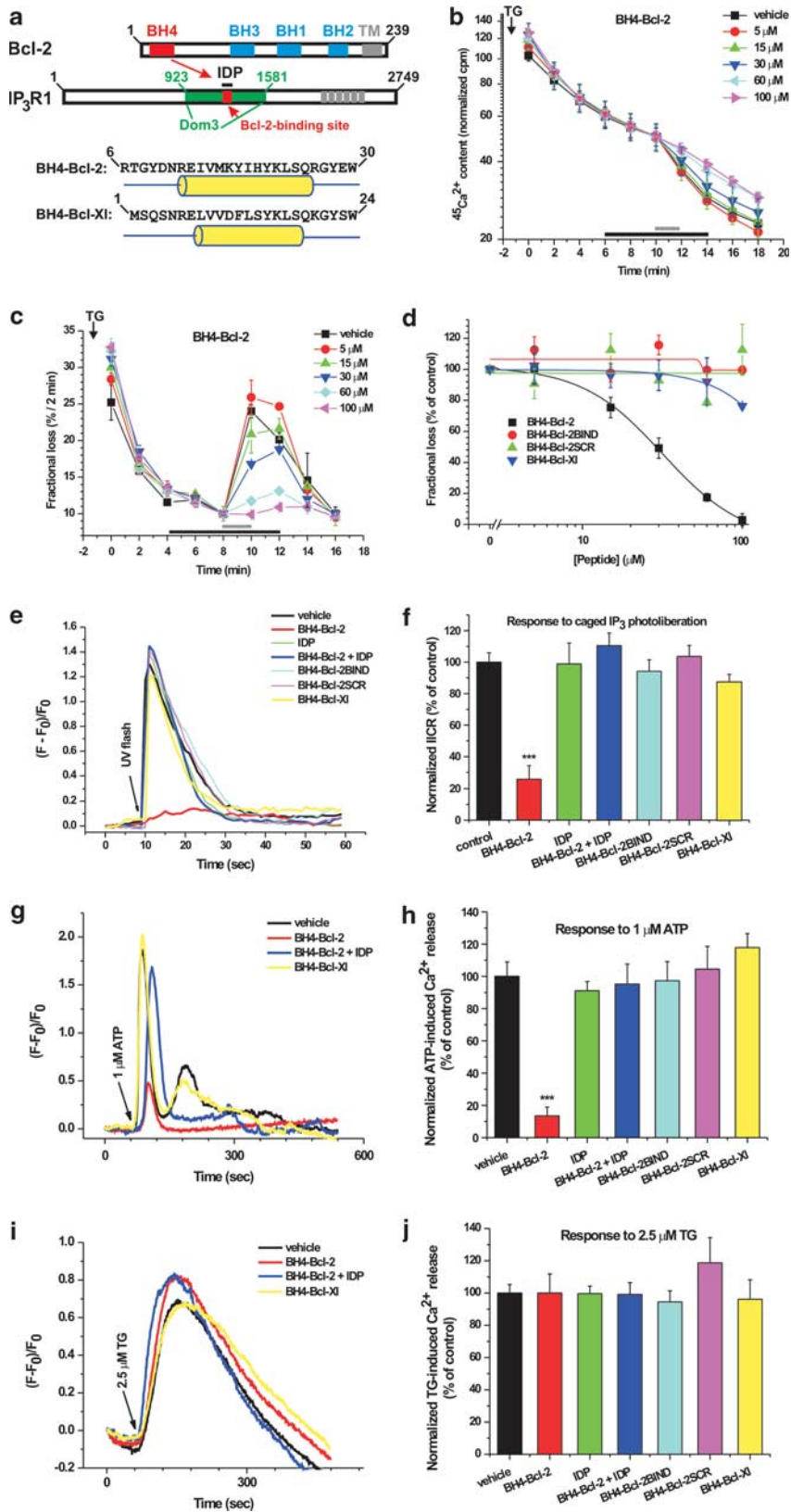
Here, we directly compared the regulation of IP_3Rs by the BH4 domains of Bcl-2 and Bcl-XI. Our results indicate that although the BH4 domain of Bcl-2 and Bcl-XI are very similar in sequence and structure, a difference in one single residue between BH4-Bcl-2 and BH4-Bcl-XI critically determined its IP_3R binding, suppression of IP_3R activity and protection against IP_3R -driven apoptosis.

Results

BH4-Bcl-2 and BH4-Bcl-XI differentially regulate IICR. The structure of antiapoptotic Bcl-2 and of a monomeric subunit of the $\text{IP}_3\text{R1}$ is depicted in Figure 1a,

including the interaction of Bcl-2 via its BH4 domain with the $\text{IP}_3\text{R1}$. The IP_3R -derived peptide (IDP; a.a. 1389–1408) corresponds to the Bcl-2-binding site on $\text{IP}_3\text{R1}$ and is therefore able to disrupt Bcl-2/ IP_3R interaction in a competitive way. IDP completely alleviates the inhibitory action of the BH4 domain of Bcl-2 on IP_3Rs without affecting other BH4-domain targets, like voltage-dependent anion channel (VDAC) and calcineurin.²⁹ Thus, IDP is an excellent tool to decipher the role of IP_3R in the observed actions of BH4-Bcl-2 on intracellular Ca^{2+} signaling and cell death. Here, we directly compared the effect of BH4-Bcl-2 and BH4-Bcl-XI on IICR using a unidirectional $^{45}\text{Ca}^{2+}$ -flux assay in saponin-permeabilized mouse embryonic fibroblasts (MEF cells) in which the non-mitochondrial Ca^{2+} stores were loaded to steady state with $^{45}\text{Ca}^{2+}$. After adding 4 μM thapsigargin (TG), the efflux of $^{45}\text{Ca}^{2+}$ was followed in the presence of 1 mM ethylene glycol tetraacetic acid (EGTA). This assay allows the quantitative assessment of Ca^{2+} -efflux properties under unidirectional conditions in the absence of ER and mitochondrial Ca^{2+} -uptake activity. Ca^{2+} content (Figure 1b) and fractional loss (Figure 1c) were plotted as a function of time. Figure 1b shows that because of an inherent Ca^{2+} leak, the Ca^{2+} content of the stores slowly decreased over time, whereas adding IP_3 (3 μM) accelerated the decrease in Ca^{2+} content due to IICR, observed as a steep increase in the fractional loss (Figure 1c). The BH4 domains of Bcl-2 (BH4-Bcl-2; a.a. 6–30) and Bcl-XI (BH4-Bcl-XI; a.a. 1–24) were produced as synthetic peptides. A scrambled version of the BH4 domain of Bcl-2 (BH4-Bcl-2SCR) and a 'binding-deficient' version of BH4-Bcl-2, in which the surface-accessible residues were altered (BH4-Bcl-2BIND),³⁰ were used as negative controls. The $^{45}\text{Ca}^{2+}$ -flux assays showed that BH4-Bcl-2 caused a potent concentration-dependent inhibition of IICR (Figures 1b and c). Importantly, BH4-Bcl-2 did not alter the Ca^{2+} -leak rate from the ER in the absence of IP_3 . In contrast to BH4-Bcl-2, BH4-Bcl-2BIND and BH4-Bcl-2SCR did not inhibit IICR (Figure 1d and Supplementary Figures 1A and B). BH4-Bcl-2 inhibited IICR with a half-maximal inhibitory concentration (IC_{50}) of $\sim 30 \mu\text{M}$ and an IC_{100} of $\sim 100 \mu\text{M}$ (Figure 1d). Strikingly, BH4-Bcl-XI did not inhibit IICR (estimated $\text{IC}_{50} > 500 \mu\text{M}$)

Figure 1 Although the BH4 domains of Bcl-2 and Bcl-XI are similar in sequence and structure, they differentially regulate IP_3R -mediated Ca^{2+} flux in permeabilized and intact cells. (a) Schematic presentation of the antiapoptotic Bcl-2-family members and the IP_3R . The N-terminal BH4 domain is unique for antiapoptotic members. The secondary structure and primary sequence of BH4-Bcl-2 and BH4-Bcl-XI are very similar. The cylindrical tube represents the predicted α -helical structure (PSIPREDv2.7). The central modulatory domain of the $\text{IP}_3\text{R1}$, containing the Bcl-2-binding site (a.a. 1389–1408), is depicted (Dom3 = a.a. 923–1581). A peptide corresponding to a.a. 1389–1408 (IDP) could prevent binding of Bcl-2 to IP_3Rs . (b) Unidirectional $^{45}\text{Ca}^{2+}$ fluxes in permeabilized MEF cells plotted as $^{45}\text{Ca}^{2+}$ content (counts per min (c.p.m.)) as a function of time (min). Ca^{2+} release was activated by 3 μM IP_3 (gray bar) in the absence or presence of the different BH4-domain peptides (black bar). A typical experiment is shown. (c) Same experiment as in (b), but results are plotted as fractional loss (%/2 min) as a function of time. (d) IICR was quantified as the fractional loss after 2 min of IP_3 incubation minus the fractional loss before the IP_3 addition. IICR in the presence of vehicle was set as 100% and other values were normalized to this value. A dose-response curve is shown for BH4-Bcl-2, a non-binding mutant of BH4-Bcl-2 (BH4-Bcl-2BIND), BH4-Bcl-2 SCR and BH4-Bcl-XI, obtained from three to four independent experiments. Data points represent mean \pm S.E.M. (e) Intracellular Ca^{2+} signals in intact C6 glioma cells were monitored using Fluo-3. Cells were loaded with caged IP_3 (50 μM) and electroporated with different BH4-domain peptides (20 μM) and/or IDP. IP_3 was released by a UV flash and a rapid increase in cytosolic $[\text{Ca}^{2+}]$ was observed. (f) Quantitative analysis of the area under the curve in (e) was obtained from at least six independent experiments and data are plotted as mean \pm S.E.M. These data indicate that BH4-Bcl-2 significantly inhibited IICR, whereas the other BH4-domain peptides did not. IDP (20 μM) prevented the inhibition of IICR by BH4-Bcl-2. (g) A typical experiment in Fluo-3-loaded C6 glioma cells loaded with 20 μM of different BH4-domain peptides or IDP depicting Ca^{2+} signals in response to ATP (1 μM). For clarity reasons, Ca^{2+} responses in cells loaded with vehicle, BH4-Bcl-2, BH4-Bcl-2 + IDP or BH4-Bcl-XI are shown. (h) Quantitative analysis of the area under the curve of the ATP-induced Ca^{2+} signals in intact Fluo-3-loaded C6 glioma cells loaded with the different BH4-domain peptides (20 μM) in response to 1 μM ATP (5–9 independent experiments). (i) Similar experiment as (g) except that cells were pretreated with EGTA (1 mM) 1 min before exposure to thapsigargin (TG; 2.5 μM). (j) Quantitative analysis of the area under the curve of the TG-induced Ca^{2+} responses (five independent experiments)



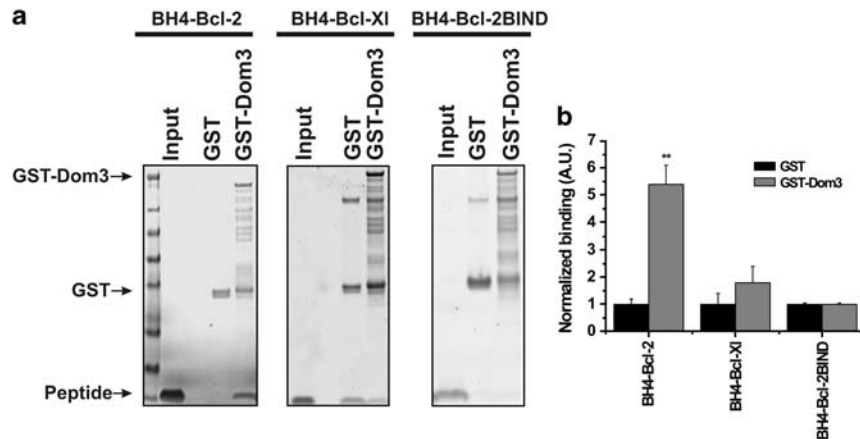


Figure 2 A GST-fusion protein corresponding to the central, modulatory domain of IP₃R1 binds BH4-Bcl-2, but not BH4-Bcl-XI or BH4-Bcl-2BIND. (a) GST pull-down assays were used for assessing the binding of BH4-Bcl-2, BH4-Bcl-XI or BH4-Bcl-2 BIND to either GST or GST-Dom3. Samples were analyzed via SDS-PAGE and total protein was stained. Bands corresponding to the BH4-domain peptides were quantified using ImageQuant. (b) The results of 3–7 independent experiments are plotted as mean \pm S.E.M. **Significantly different from GST control ($P < 0.01$)

(Figure 1d and Supplementary Figure 1C). We repeated the experiments using more physiological conditions, like 300 nM free Ca²⁺ (Supplementary Figure 2B), 1 μ M free Ca²⁺ (Supplementary Figure 2C) and 1 mM Mg-ATP (Supplementary Figure 2D), and found that 40 μ M BH4-Bcl-2 equally inhibited IICR.

Next, we examined the differential regulation of IP₃Rs by BH4-Bcl-2 and BH4-Bcl-XI in C6 glioma cells, a cellular model optimized for *in situ* electroporation of membrane-impermeable molecules.^{32,33} We loaded BH4-Bcl-2 or BH4-Bcl-XI (both 20 μ M) by electroporation and found that BH4-Bcl-2 inhibited IICR triggered by IP₃ photoliberation from its caged precursor in intact C6 cells (50 μ M; Figures 1e and f), whereas BH4-Bcl-XI did not. BH4-Bcl-2SCR and BH4-Bcl-2BIND control peptides did not reduce IICR. The inhibition by BH4-Bcl-2 was completely prevented by loading the cells with IDP (20 μ M), indicating a competitive binding of BH4-Bcl-2 to IP₃Rs. Similar results were obtained using adenosine 5'-triphosphate (ATP; 1 μ M), a physiological agonist provoking IP₃R-mediated Ca²⁺ release in these cells (Figures 1g and h). Finally, we assessed the TG (2.5 μ M)-releasable Ca²⁺ in these cells 1 min after exposing the cells to EGTA (1 mM) and found no differences among the different conditions (Figures 1i and j). Hence, the decreased ATP-induced Ca²⁺ release in the presence of BH4-Bcl-2 was not because of decreased ER Ca²⁺-store content.

These results indicate that BH4-Bcl-2 and BH4-Bcl-XI differentially regulate IP₃R function independently of the ER Ca²⁺-store content.

BH4-Bcl-2 and BH4-Bcl-XI differentially bind to the central domain of the IP₃R. Next, we compared the binding of BH4-Bcl-2 and BH4-Bcl-XI with glutathione-S-transferase (GST)-Dom3 (i.e. a.a. 923–1581 of IP₃R1; Figures 2a and b). Using GST pull-down assays, we found that BH4-Bcl-2, but not BH4-Bcl-XI, strongly and specifically interacted with GST-Dom3. However, we consistently

noticed a higher nonspecific binding of BH4-Bcl-XI to GST than for BH4-Bcl-2. The reason for this is unclear. BH4-Bcl-2BIND was not pulled down by GST-Dom3 (Figures 2a and b), indicating that surface-accessible residues are important for interaction with IP₃Rs.

We also assessed the binding of GST-Dom3 to BH4-Bcl-2 and BH4-Bcl-XI in a more quantitative manner using surface plasmon resonance (SPR). We monitored the binding of GST-Dom3 (Figures 3a–c) and GST (Supplementary Figures 3A–C and Figure 3e) to the streptavidin-coated sensor chip containing immobilized biotinylated peptides. Background signals obtained from the reference flow cell containing the scrambled peptides were subtracted to generate response curves. In each sensorgram, the association phase is plotted. GST (up to 40 μ M) bound to neither biotin-BH4-Bcl-2 nor biotin-BH4-Bcl-XI (Supplementary Figures 3A–C). GST-Dom3 displayed a concentration-dependent increase in resonance units, in the biotin-BH4-Bcl-2-containing flow cell (Figure 3a). This indicates a specific binding toward biotin-BH4-Bcl-2 with estimated dissociation constant (K_d) of ~ 1 μ M (Figure 3c). In the biotin-BH4-Bcl-XI-containing flow cell (Figure 3b), GST-Dom3 resulted in significantly less increase in resonance units (Figure 3c).

We also monitored the binding of GST-Dom3 to biotin-BH4-Bcl-2BIND corrected for the response to the scrambled counterpart (Figure 3d). Clearly, GST-Dom3 did not specifically bind to biotin-BH4-Bcl-2BIND. The negative values in the sensorgrams indicate a slightly higher binding of GST-Dom3 to the scrambled version.

As the Bcl-2-binding site²⁸ is largely conserved among the different IP₃R isoforms, we compared the BH4-Bcl-2-binding properties of the GST-Dom3 (3.3 μ M) derived from IP₃R1, IP₃R2 and IP₃R3 (Figures 3e and f). GST-Dom3 from all three IP₃R isoforms bound to biotin-BH4-Bcl-2 with roughly similar potencies (Figures 3e and f). The quality of the purified GST-fusion proteins was controlled using sodium dodecyl sulfate-polyacrylamide gel electrophoresis (SDS-PAGE; Figure 3g).

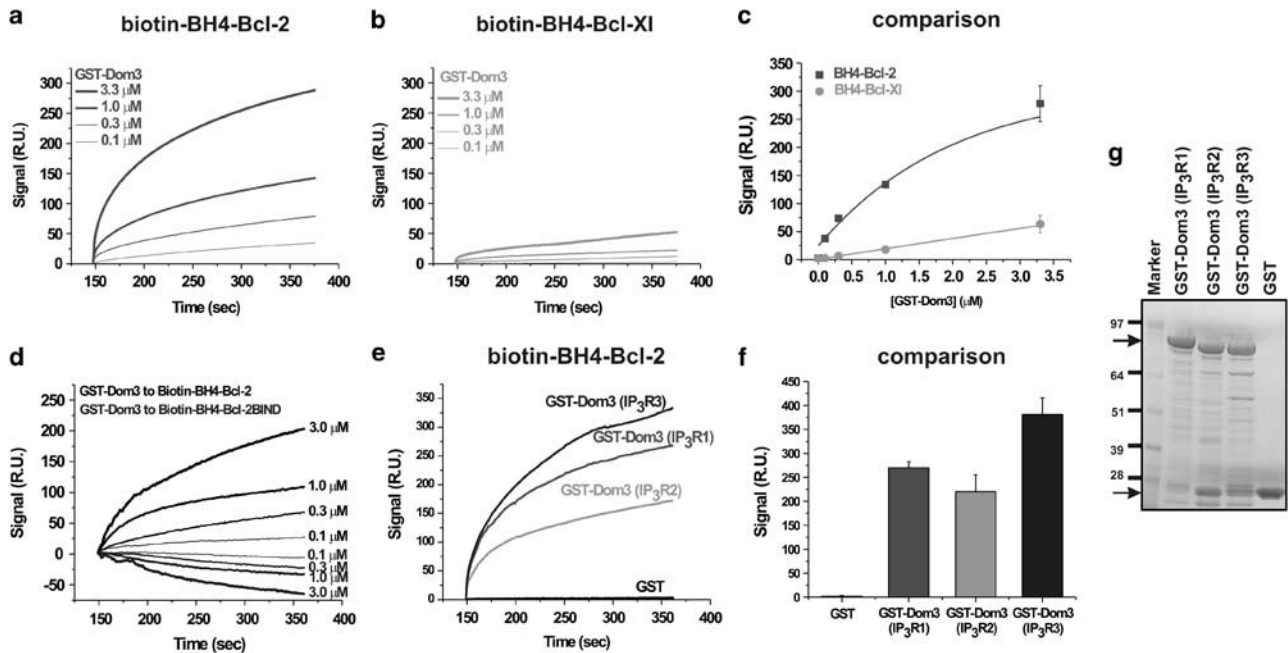


Figure 3 The central, modulatory domain of IP₃R1 binds to immobilized biotin-BH4-Bcl-2, but not to biotin-BH4-Bcl-Xl, in SPR experiments. (a–c) Sensorgrams are obtained after background correction for binding to the respective scrambled versions of the biotinylated BH4-domain peptides. The association phase is shown upon addition of different concentrations of purified GST-Dom3 to biotin-BH4-Bcl-2 (a) or biotin-BH4-Bcl-Xl (b). A typical experiment is shown. (c) The quantitative analysis of the binding properties of GST-Dom3 to either biotin-BH4-Bcl-2 or biotin-BH4-Bcl-Xl is shown. Values were obtained from three independent experiments and are plotted as mean ± S.E.M. (d) Sensorgrams representing the association phase of different concentrations of GST-Dom3 for the binding to either biotin-BH4-Bcl-2 or biotin-BH4-Bcl-2BIND. All curves are background corrected for binding to the respective scrambled peptides. (e) Sensorgrams representing the binding of purified GST-Dom3 (3.3 μM) obtained from IP₃R1, IP₃R2 and IP₃R3 to biotin-BH4-Bcl-2. GST (3.3 μM) was included as a control. (f) Quantitative analysis of the binding of purified GST and GST-Dom3 obtained from IP₃R1, IP₃R2 and IP₃R3 (all at 3.3 μM) to biotin-BH4-Bcl-2. Values were obtained from three independent experiments and are plotted as mean ± S.E.M. (g) A representative GelCode Blue-stained 4–12% Bis-Tris NUPAGE gel run in MOPS-SDS buffer showing the quality of the purified GST and GST-Dom3 derived from IP₃R1, IP₃R2 and IP₃R3 used in these SPR experiments. The upper arrow indicates the full-length GST-IP₃R-fusion proteins, whereas the lower arrow indicates parental GST.

Identification of residues in BH4-Bcl-2 responsible for inhibiting IP₃Rs. Next, we investigated which residues in BH4-Bcl-2 are responsible for interaction with IP₃Rs. Based on a bioinformatics approach,³⁰ we successively changed the various predicted surface-accessible residues into alanines (Figure 4a) and investigated their properties toward inhibiting IICR as described in Figure 1. We applied 60 μM of the different BH4-Bcl-2 mutant peptides. This concentration, when used for wild-type BH4-Bcl-2, reduced the IICR to ~20% of its control value (Figure 4b). This analysis revealed that BH4-Bcl-2 acts as a discontinuous binding domain, in which every surface-accessible residue (Asp10, Arg12, Lys17, His20, Tyr21, Gln25, Arg26, Tyr28) contributed to the inhibition of IICR. In particular, Lys17, His20, Tyr21 or Arg26 seemed critical for the inhibitory properties of BH4-Bcl-2. Moreover, changing these residues into an Ala may indirectly affect the binding of BH4-Bcl-2 to IP₃Rs by altering its α-helical properties. It has to be noted that although minor changes in the secondary structure can occur, all Ala mutants displayed similar predicted α-helical properties as the wild-type BH4-Bcl-2 using PSIPRED vs3.0 (Supplementary Figure 4, <http://bioinf.cs.ucl.ac.uk/psipred/>).

Sequence alignment identifies a difference of one critical residue essential for differential IP₃R-inhibitory properties of BH4-Bcl-2 and BH4-Bcl-Xl. Sequence

alignment shows that Lys17 (K17) in BH4-Bcl-2 corresponds to Asp11 (D11) in BH4-Bcl-Xl (Figure 5a), thereby introducing a charge change in the middle of the α-helical structure.^{29,34,35} Hence, we made a mutant BH4-Bcl-2 peptide in which we replaced Lys17 by an aspartate (BH4-Bcl-2 K/D) and a mutant BH4-Bcl-Xl peptide in which we replaced Asp11 by a lysine (BH4-Bcl-Xl D/K). Strikingly, we found that BH4-Bcl-2 K/D failed to inhibit IICR, whereas BH4-Bcl-Xl D/K strongly reduced IICR (Figures 5b and c). Dose-response curves (Figure 5d) indicated that BH4-Bcl-2 and BH4-Bcl-Xl D/K inhibited IICR with an IC₅₀ of 30 and 60 μM, respectively. In contrast, BH4-Bcl-Xl and BH4-Bcl-2 K/D were largely ineffective. The effects of the BH4-domain mutants on IICR were also observed in intact C6 glioma cells using caged IP₃ (Figures 5e and f). In contrast to BH4-Bcl-2, BH4-Bcl-2 K/D did not inhibit IICR in intact cells, whereas in contrast to BH4-Bcl-Xl, BH4-Bcl-Xl D/K was able to significantly reduce IICR. Similar results were obtained using the physiological agonist ATP (1 μM; Figure 5g), whereas none of the BH4-domain peptides did alter the amount of TG (2.5 μM)-releasable Ca²⁺ from the ER (Figure 5h).

The importance of this critical residue was underpinned by SPR experiments using immobilized biotin-BH4-Bcl-2 K/D and biotin-BH4-Bcl-Xl D/K. Consistent with the functional data, BH4-Bcl-2 K/D largely lost its ability to interact with

GST-Dom3 (Figure 5i), whereas BH4-Bcl-XI D/K was able to bind GST-Dom3 (Figure 5j).

Taken together, these data indicate that one single residue difference between BH4-Bcl-2 and BH4-Bcl-XI can explain their differential action on IP₃Rs.

BH4-Bcl-2 and BH4-Bcl-XI differentially affect apoptosis. Next, we assessed whether BH4-Bcl-2 and BH4-Bcl-XI displayed a difference in protection against apoptotic cell death in C6 glioma cells triggered by loading the cells with cytochrome *c* (CytC; 10 μM, 25 min) or by incubation with staurosporine (STS; 2 μM, 6 h). The apoptotic index (AI) was determined and expressed relative to the condition in which apoptosis was triggered in the absence of BH4 peptides (vehicle), which was set to 100%.

We first examined whether CytC interaction with the IP₃R contributed to CytC-induced apoptosis in the C6 cell model. The CytC–IP₃R interaction is part of a positive feedback loop that enhances cell death by promoting ER Ca²⁺ release through IP₃R channels.^{36,37} We examined CytC-induced cell death in the absence and presence of a peptide matching the CytC-binding site on IP₃Rs (IP3RCYT; 50 μM). Cells loaded with IP3RCYT displayed a decrease of ~50–60% in CytC-induced cell death (Figure 6a). These results indicate that part

of the CytC-induced cell death was because of CytC binding to the IP₃Rs. We tested the different BH4-domain peptides (20 μM) in this cell system and found that both BH4-Bcl-2 and BH4-Bcl-XI protected against CytC-induced cell death. However, BH4-Bcl-2 was significantly more potent in protecting than BH4-Bcl-XI (Figure 6b). The BH4-Bcl-2SCR control did not protect at all. Importantly, changing Lys17 into Asp in BH4-Bcl-2 (BH4-Bcl-2 K/D) reduced the level of protection, thereby resembling BH4-Bcl-XI. In contrast, changing Asp11 into Lys in BH4-Bcl-XI (BH4-Bcl-XI D/K) increased cell survival, thereby resembling BH4-Bcl-2.

To assess whether the difference in potency between BH4-Bcl-2 and BH4-Bcl-XI is because of their differential action on the IP₃R, the BH4-domain peptides were loaded together with IDP competing with the IP₃R for binding of Bcl-2. IDP completely abolished the protective action of BH4-Bcl-2, but not that of BH4-Bcl-XI (Figure 6c).

We also used STS, which acts upstream of the mitochondria and CytC release and initiates apoptosis via ER Ca²⁺-release-dependent mechanisms.^{38,39} STS induced apoptosis with a minor fraction of these cells displaying secondary necrosis (Figure 6d). Primary necrosis was not observed, as all propidium iodide (PI)-positive cells were also characterized by activated caspases (cysteine-dependent

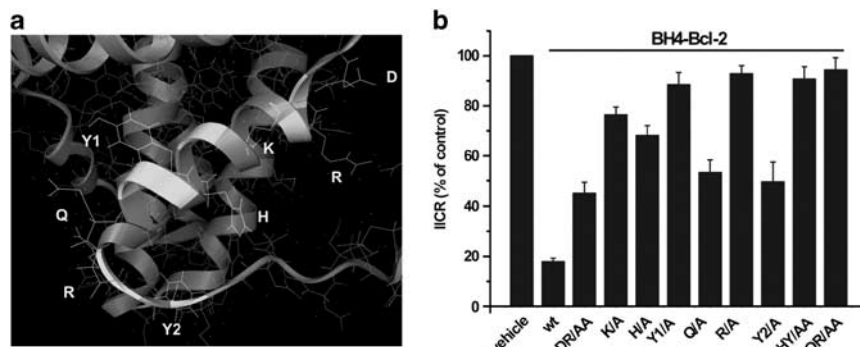
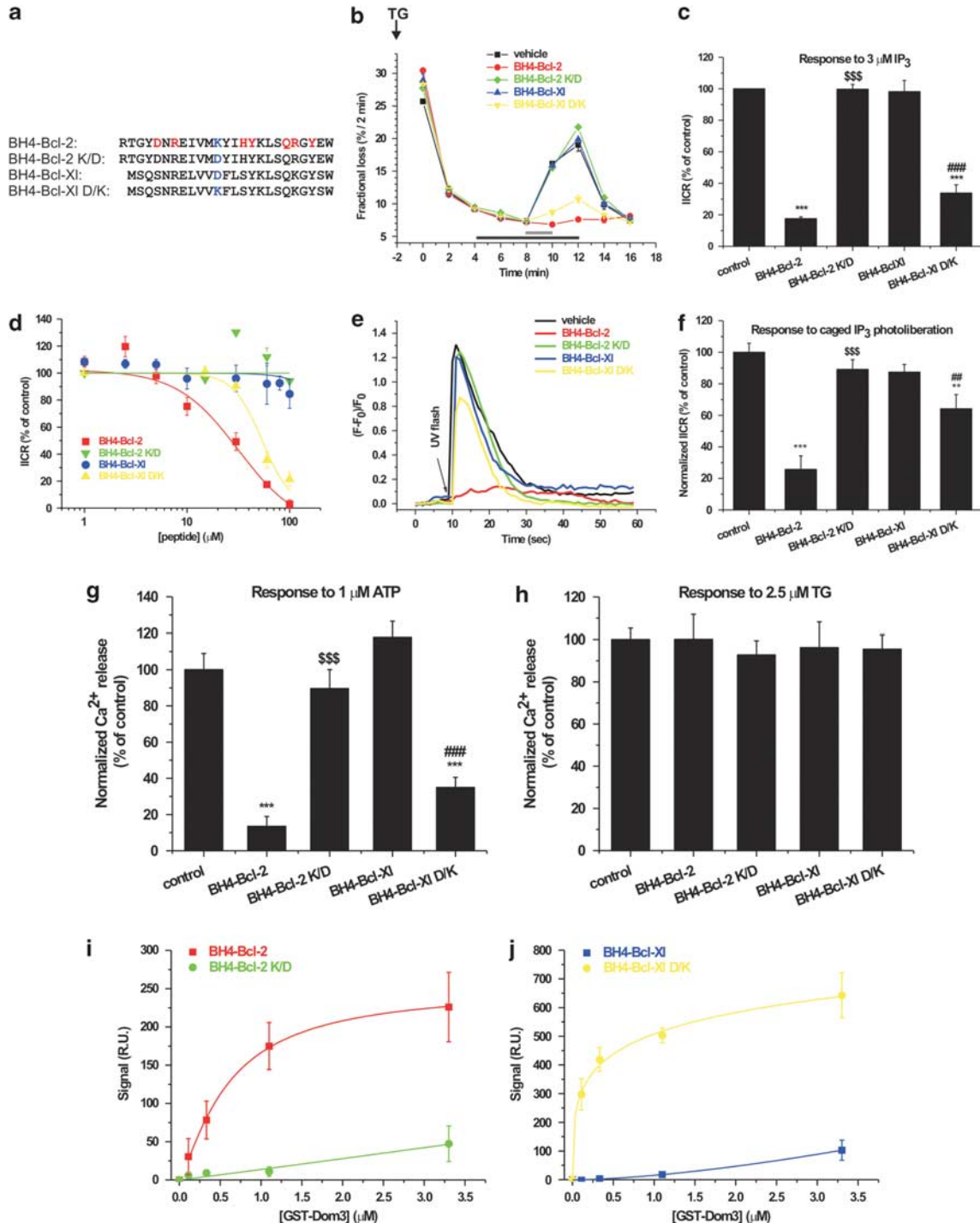


Figure 4 Determination of the residues in BH4-Bcl-2 critical for inhibiting IICR. (a) Zoomed picture of the BH4 domain of Bcl-2 showing its surface-accessible residues is depicted. (b) The inhibitory properties of different BH4-Bcl-2 mutant versions (60 μM), in which the surface-accessible residues were altered into alanines, were monitored in unidirectional ⁴⁵Ca²⁺-flux assays in permeabilized MEF cells. Four of the six single alanine mutations (K17A, H20A, Y21A and R26A) had the largest effect on the inhibitory action of the wild-type (wt) BH4-Bcl-2 domain

Figure 5 BH4-Bcl-2 and BH4-Bcl-XI differ in one critical amino acid, which determines their effect on the IP₃R. (a) Aligned sequence of the BH4 domain of Bcl-2 and Bcl-XI with indication of the surface-accessible residues (in color) is shown. The critical residue Lys17 in BH4-Bcl-2 is not conserved in BH4-Bcl-XI (depicted in blue). The sequences of these BH4-domain peptides are indicated. (b) A typical experiment of a unidirectional ⁴⁵Ca²⁺-flux assay in permeabilized MEF cells, comparing the effect of BH4-Bcl-2, BH4-Bcl-XI, BH4-Bcl-2 K/D and BH4-Bcl-XI D/K (80 μM of peptides). (c) The quantification of the effects of the different BH4-domain peptides (80 μM) on IICR was obtained from three to four independent experiments. Data points represent mean ± S.E.M. *BH4-Bcl-2 and BH4-Bcl-XI D/K are statistically different from control. [§]BH4-Bcl-2 K/D is statistically different from BH4-Bcl-2. [#]BH4-Bcl-XI D/K is statistically different from BH4-Bcl-XI. (d) A dose-response curve for the different BH4-domain peptides was obtained from three independent experiments. Values are plotted as mean ± S.E.M. (e) Representative IP₃R-mediated Ca²⁺ traces in intact C6 glioma cells using caged IP₃ and UV photoliberation. (f) Quantitative analysis of the area under the curve, of the traces in (e), was obtained from at least six independent experiments and data are plotted as mean ± S.E.M. BH4-Bcl-2 and BH4-Bcl-XI D/K significantly inhibited IICR, in contrast to BH4-Bcl-2 K/D and BH4-Bcl-XI. *BH4-Bcl-2 and BH4-Bcl-XI D/K are statistically different from control. [§]BH4-Bcl-2 K/D is statistically different from BH4-Bcl-2. [#]BH4-Bcl-XI D/K is statistically different from BH4-Bcl-XI. (g) Similar experiment as in (e and f), except that Ca²⁺ signals were elicited by ATP (1 μM). Area under the curve of different control cells was determined and set at 100%. (h) Similar experiment as in (e and f), except that cells were pretreated for 1 min with EGTA (1 mM) and exposed to thapsigargin (TG, 2.5 μM). Area under the curve for control was determined and set at 100%. Statistically significant differences were considered at *P* < 0.05 (single symbols), *P* < 0.01 (double symbols) and *P* < 0.001 (triple symbols). (i) Quantitative analysis of data obtained from three independent SPR experiments, in which the binding of different concentrations of GST-Dom3 to immobilized biotin-BH4-Bcl-2 was compared with its binding to immobilized biotin-BH4-Bcl-2 K/D. The maximal signal (resonance units) during the association phase was used in this analysis. (j) Quantitative analysis of data obtained from SPR experiments, in which the binding of GST-Dom3 to biotin-BH4-Bcl-XI was compared with its binding to biotin-BH4-Bcl-XI D/K. The maximal signal (resonance units) during the association phase was used in this analysis

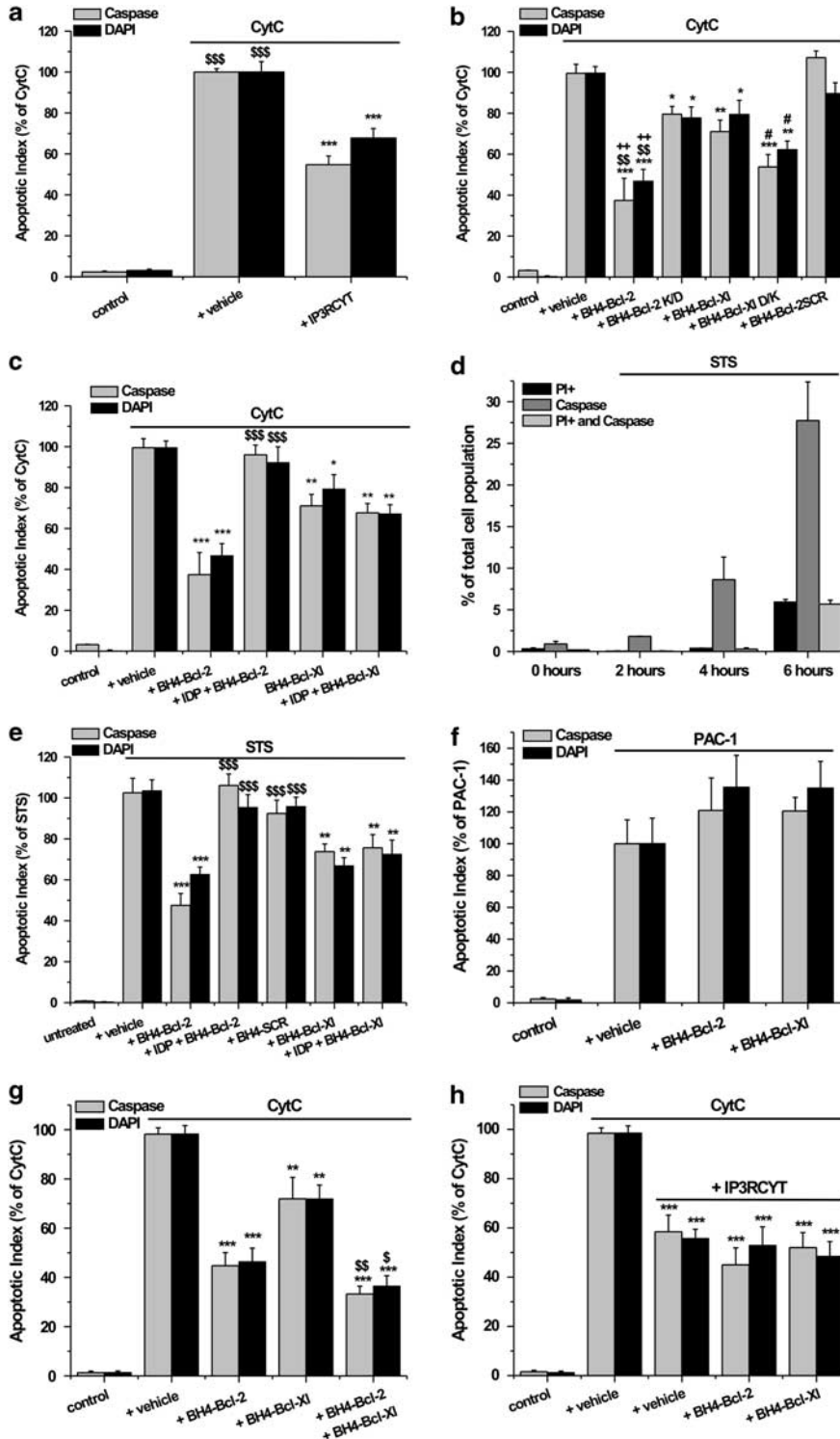
aspartate-specific proteases). Results with STS were similar to those obtained with CytC loading (Figure 6e). Both BH4-Bcl-2 and BH4-Bcl-Xl, but not BH4-Bcl-2SCR, protected against STS-induced cell death. However, BH4-Bcl-2 was significantly more potent than BH4-Bcl-Xl. BH4-Bcl-2-mediated protection against STS was completely suppressed by IDP, whereas the effect of BH4-Bcl-Xl was independent of IDP.

As an additional control, we used first procaspase activating compound (PAC-1; 150 μ M, 6h), a direct procaspase-3 activating compound downstream of CytC.⁴⁰ These conditions caused apoptosis in \sim 15% of the cell population. We found that BH4-Bcl-2 and BH4-Bcl-Xl did not protect against PAC-1-induced cell death, confirming that the target of these peptides is indeed upstream of caspase-3 (Figure 6f).



Co-loading of BH4-Bcl-2 with BH4-Bcl-Xl in C6 glioma cells did not display an additive effect toward their protection against CytC- and STS-induced cell death (Figure 6g and Supplementary Figure 5). The protective effects of both BH4-Bcl-2 and BH4-Bcl-Xl against CytC-induced apoptosis were ablated when the positive feedback loop of CytC on the IP₃R was prevented by co-loading IP3RCYT peptide (Figure 6h).

Collectively, these data indicate that the BH4 domains of Bcl-2 and Bcl-Xl both protect against apoptosis by acting on different targets upstream of caspase activation. Although the protective effect of BH4-Bcl-2 was stronger and largely dependent on its interaction with a specific binding site on the IP₃R, the protective effect of BH4-Bcl-Xl is independent of binding to the IP₃R. Nevertheless, in these paradigms



BH4-Bcl-XI likely acts on a target that functions downstream of the IP₃R-signaling cascade.

Full-length Bcl-2 K/D is less efficient in binding IP₃Rs, inhibiting IP₃R activity and protecting against Ca²⁺-dependent apoptosis. Finally, we tested whether the critical Lys17 identified in BH4-Bcl-2 plays a crucial role in the IP₃R-inhibitory action of full-length Bcl-2. Therefore, we mutated Lys17 into Asp in full-length 3xFLAG-Bcl-2, creating 3xFLAG-Bcl-2 K/D.

First, we compared the GST-Dom3-binding properties of 3xFLAG-Bcl-2 and 3xFLAG-Bcl-2 K/D by expressing these proteins in COS-1 cells and using GST pull-down assays (Figure 7a). We found that the binding of 3xFLAG-Bcl-2 K/D to GST-Dom3 was severely compromised compared with wild-type 3xFLAG-Bcl-2 (Figure 7b).

Next, we examined the effect of 3xFLAG-Bcl-2 and 3xFLAG-Bcl-2 K/D overexpression in COS-1 cells on ATP-induced Ca²⁺ release. We applied 1 μM ATP, a submaximal concentration for triggering Ca²⁺ signals, in Fura-2-loaded COS-1 cells. We monitored the Ca²⁺ signals in mCherry-transfected cells (Supplementary Figure 6). In each experiment, 10 cells were selected and calibrated Ca²⁺ signals were obtained. Typical Ca²⁺ responses in empty vector-, 3xFLAG-Bcl-2- and 3xFLAG-Bcl-2 K/D-transfected cells are shown in Figures 7c–e, respectively. Cells expressing 3xFLAG-Bcl-2 displayed blunted ATP-triggered Ca²⁺ signals in comparison with empty vector- or 3xFLAG-Bcl-2 K/D-transfected cells (Figure 7f). 3xFLAG-Bcl-2 was much more potent in inhibiting IP₃R-mediated Ca²⁺ signals than 3xFLAG-Bcl-2 K/D (Figure 7f). In addition, there was no difference for TG-induced Ca²⁺ signals (Figure 7g). Finally, we examined the effect of 3xFLAG-Bcl-2 and 3xFLAG-Bcl-2 K/D overexpression on the protection against STS-induced apoptosis. We used the cleavage of poly-(ADP-ribose)-polymerase (PARP), a downstream target of activated caspase-3, to monitor STS-induced apoptosis in transfected COS-1 cells (Figure 7h). Compared with control cells, 3xFLAG-Bcl-2 significantly reduced PARP cleavage upon STS treatment. 3xFLAG-Bcl-2 K/D was much less potent than

3xFLAG-Bcl-2 in preventing STS-induced PARP cleavage (Figure 7i).

We confirmed these findings in WEHI7.2 cells, which contain very low Bcl-2 levels. We created stable WEHI7.2 cell lines expressing either Bcl-2 or Bcl-2 K/D. First, western blotting analysis revealed that both stable cell lines displayed similar levels of Bcl-2 and Bcl-2 K/D (Figure 8a). Next, we monitored apoptosis by western blotting analysis with PARP antibodies (Figure 8b), annexin V-fluorescein isothiocyanate (FITC)/PI fluorescence-activated cell sorting (FACS) analysis (Figures 8c and d) and caspase-3-activity assay (Figure 8e). In all assays, Bcl-2 overexpression protected WEHI7.2 cells against STS-induced apoptosis, whereas Bcl-2 K/D was less effective than wild-type Bcl-2. These data correlate well with the IP₃R-binding and Ca²⁺-signaling results obtained in COS-1 cells. Hence, Lys17 seems an important residue in the BH4 domain of full-length Bcl-2 for mediating Bcl-2-dependent inhibition of IP₃R-mediated Ca²⁺ signals and protection against STS-induced cell death.

Discussion

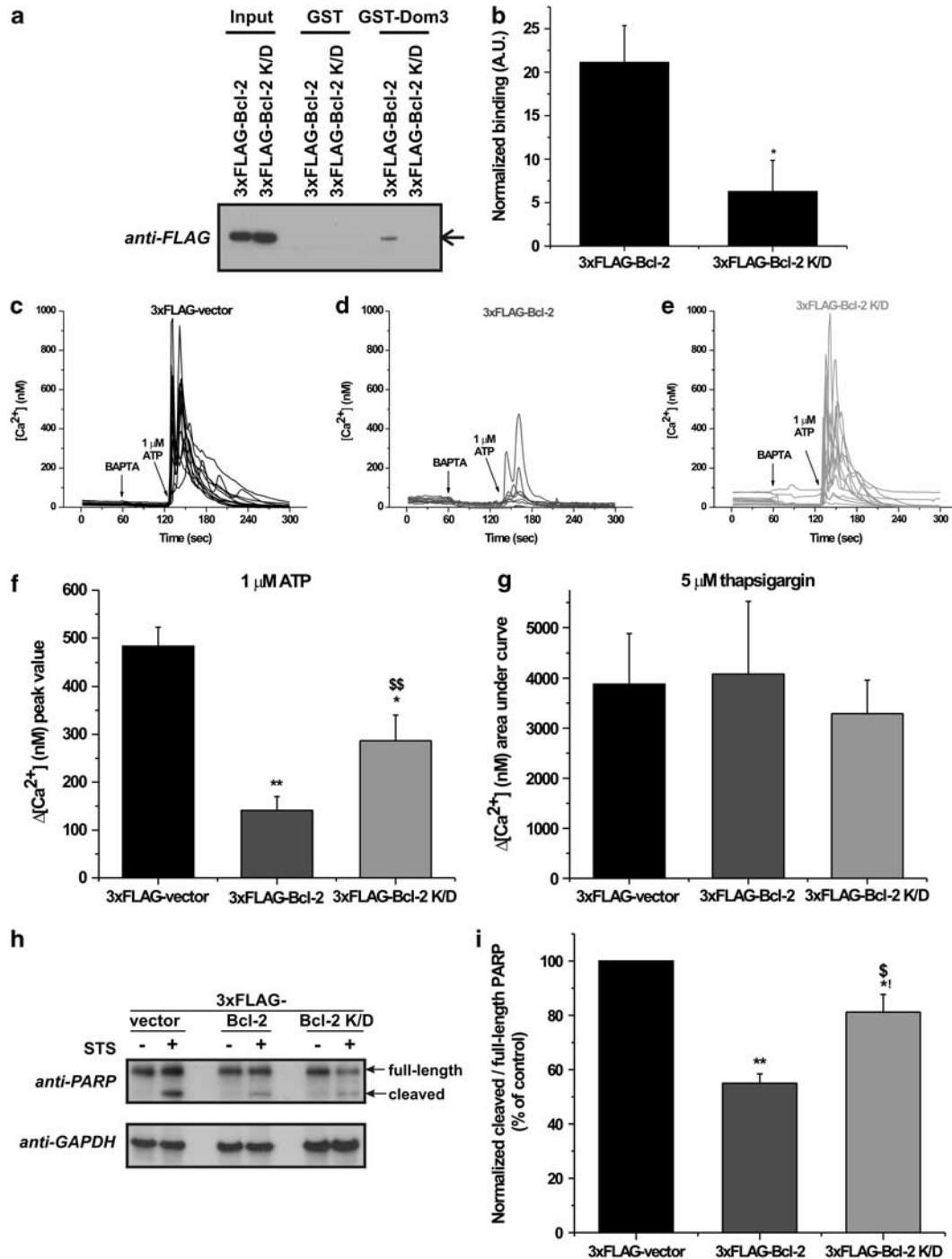
The major findings of this study are that (1) BH4-Bcl-2 and BH4-Bcl-XI, although very similar in primary sequence and secondary structure,^{29,34,35} act differentially on IP₃Rs, IICR and Ca²⁺-dependent apoptosis; (2) one critical residue that has an opposite charge in BH4-Bcl-2 *versus* BH4-Bcl-XI is responsible for their distinct biological properties; and (3) mutating this residue in the BH4 domain of full-length Bcl-2 decreases its ability to bind and inhibit IP₃Rs and to protect against apoptotic stimuli. We pinpointed one residue critical for inhibiting IP₃Rs in the sequence of BH4-Bcl-2 (Lys17) that was not conserved in BH4-Bcl-XI (Asp11). This residue is of key importance for the specific action of BH4-Bcl-2 on the IP₃R. Changing Asp11 in BH4-Bcl-XI into a Lys induced IP₃R binding and inhibition, leading to a BH4-Bcl-2-like function.

Bcl-2 and Bcl-XI both act at the mitochondrial and the ER membranes, where they regulate ER Ca²⁺ dynamics via interaction with the IP₃R.^{20–23,26} Several reports suggested that Bcl-2 predominantly inhibits proapoptotic Ca²⁺ transients, whereas Bcl-XI predominantly stimulates

Figure 6 BH4-Bcl-2, but not BH4-Bcl-XI, protects against CytC- and STS-induced apoptosis via its interaction with the IP₃R. (a–c) Loading of CytC (10 μM) in C6 glioma cells provoked a dramatic increase in the number of caspase-positive cells and cells with a fragmented nucleus (both quantified 25 min later) compared with cells loaded with buffer only (\$ in (a) indicates that CytC significantly increases the apoptotic index compared with the control loading condition lacking CytC; the significance indication for CytC *versus* control was omitted from the other panels for clarity reasons). All results were obtained from four to eight independent experiments and are plotted as mean ± S.E.M. Statistically significant differences are indicated as in Figure 5. (a) Co-loading of the IP₃R peptide corresponding to the CytC-binding site (IP3RCYT 50 μM) together with CytC significantly (*) reduced the apoptotic index, indicating that CytC-induced apoptosis was amplified by its action on the IP₃R. (b) BH4-Bcl-2, BH4-Bcl-2 K/D, BH4-Bcl-XI and BH4-Bcl-XI D/K (20 μM) significantly (*) protected against CytC-induced apoptosis in both assays, but not BH4-Bcl-2SCR. However, BH4-Bcl-2 was significantly (\$) more potent than BH4-Bcl-XI. Furthermore, Bcl-2 is significantly more potent than Bcl-2 K/D (+), whereas Bcl-XI D/K is significantly more potent than BH4-Bcl-XI (#). (c) BH4-Bcl-2-mediated protection against CytC-induced apoptosis was alleviated by co-loading with 20 μM IDP, whereas the antiapoptotic activity of BH4-Bcl-XI was not affected by IDP. Thus, BH4-Bcl-2, BH4-Bcl-XI and BH4-Bcl-XI + IDP significantly (*) reduced CytC-induced apoptosis, but not BH4-Bcl-2 + IDP. Furthermore, BH4-Bcl-2 + IDP is significantly (\$) different from BH4-Bcl-2. (d) Characterization of the STS (2 μM)-induced cell death profile by analyzing the percentage of cells staining positive for propidium iodide (PI +), caspase activation (Caspase) and both PI and caspase activation (PI + and Caspase) as a function of time. (e) Similar approach as in (c) but with STS as an apoptotic trigger (applied in the medium for 6 h at 2 μM). (f) Similar approach as in (a–c), but with PAC-1, a small molecular activator of caspase-3, as an apoptotic trigger (applied in the medium for 6 h at 150 μM). (g) Effect of combining BH4-Bcl-2 and BH4-Bcl-XI (both 20 μM) on CytC-induced apoptosis. *All conditions significantly reduced CytC-induced apoptosis. \$The combination of BH4-Bcl-2 and BH4-Bcl-XI is significantly different from BH4-Bcl-XI, but not from BH4-Bcl-2. These results indicate no additive effect by combining BH4-Bcl-2 with BH4-Bcl-XI. (h) Effect of BH4-Bcl-2 and BH4-Bcl-XI on CytC-induced apoptosis in the presence of IP3RCYT peptide. *All conditions significantly reduced CytC-induced apoptosis. However, the protective effects of both BH4-Bcl-2 and BH4-Bcl-XI were ablated in the presence of IP3RCYT peptide (50 μM) and thus did not significantly differ from the vehicle-treated condition

IP₃R-mediated prosurvival Ca²⁺ oscillations.^{21–23,26,28} Nevertheless, other reports showed that Bcl-2 too may enhance IP₃R activity^{20,25} and/or stimulate Ca²⁺ oscillations.^{21,41} Hence, until now, it was not clear whether Bcl-2 and Bcl-XI displayed distinct functional properties toward regulating IP₃R and thus Ca²⁺-regulated apoptosis or whether they were similar in their action. As we recently showed that BH4-Bcl-2 was sufficient to protect against IP₃R-mediated apoptosis, we now made a direct comparison of the BH4-domain properties of

Bcl-2 and Bcl-XI by using synthetic peptides. Our study reveals a specific cellular function for the BH4 domain of Bcl-2 as a potent inhibitor of IICR and Ca²⁺-dependent apoptosis, which is not shared by the BH4 domain of Bcl-XI, although both motifs are very similar in sequence and structure. Our data indicate that this is because of a critical charge difference in one of the surface-accessible amino-acid residues. As a result, BH4-Bcl-XI did not inhibit Ca²⁺ flux through the IP₃R. Nevertheless, BH4-Bcl-XI protected against cell death.



However, this effect was significantly smaller than for BH4-Bcl-2 and was not due to inhibition of IICR. This was concluded from the observation that IDP counteracting the effect of BH4-Bcl-2 did not interfere with the protective function of BH4-Bcl-XI. Finally, using exogenous expression in COS-1 and WEHI7.2 cells, we demonstrated that the role of Lys17 is important for the action of full-length Bcl-2 on the IP₃R, as full-length Bcl-2 K/D was much less efficient in binding and inhibiting IP₃Rs as well as in protecting against apoptotic stimuli. We observed a weak binding of full-length Bcl-2 K/D (i.e. ~20% of the binding of wild-type Bcl-2) to the IP₃R fragment, which indicates that residues other than Lys17 may contribute to the binding of full-length Bcl-2 to the IP₃R. This remaining binding of Bcl-2 K/D to IP₃R may be responsible for the weak inhibitory property of this protein on IP₃R-mediated Ca²⁺ signaling and its protective effects against STS-induced apoptosis. However, the latter may also be related to the antiapoptotic actions of Bcl-2 K/D through its hydrophobic cleft and may therefore suggest that its ability to scaffold proapoptotic BH3-domain proteins is unaffected by this mutation in the BH4 domain.

Clearly, whereas Bcl-2 exclusively interacts with the central domain of the IP₃R,²⁸ Bcl-XI seems to interact with the C-terminal tail of the IP₃R.²³ The latter domain has been proposed to contain two putative BH3-like domains and may therefore interact with the hydrophobic cleft of Bcl-XI.²⁴

Besides the differential interaction with the IP₃R, Bcl-2 and Bcl-XI could also differ with respect to other previously identified targets of the BH4 domain of Bcl-2-family members, as calcineurin, VDAC, RAF-1 (v-raf-1 murine leukemia viral oncogene homolog 1), RAS (RAt Sarcoma), CED (cell death abnormal)-4, paxillin and NF-κB (nuclear factor kappa-light-chain enhancer of activated B cells), all of which may play a role in apoptosis.³⁰ A side-by-side comparison between Bcl-2 and Bcl-XI will be required to examine whether there is a distinct or preferential action of either domain on these targets and whether the critical sequence difference between BH4-Bcl-2 and BH4-Bcl-XI revealed in this study affects their activity or selectivity. Furthermore, considering the preferential targeting of Bcl-XI to the mitochondrial outer membrane,⁴² we speculate that the protective action of BH4-Bcl-XI may be mediated by modulating mitochondrial targets.⁴³ Although BH4-Bcl-2 and BH4-Bcl-XI appear to have distinct targets, these targets likely do not function in completely independent pathways. Indeed, a combination of BH4-Bcl-2 and BH-Bcl-XI

did not provoke an additive protective effect and IP3RCYT abolished the protective effect of both BH4-Bcl-2 and BH4-Bcl-XI against CytC-induced apoptosis. Thus, Bcl-XI may act through its BH4 domain on a target downstream of the IP₃R, whereas other targets independently of the IP₃R/Ca²⁺-signaling cascade cannot be excluded.

Our study may have important therapeutic consequences for cancers dependent on high levels of Bcl-2, like chronic lymphocytic leukemia.^{44,45} It may be possible to target the BH4 domain of Bcl-2 in these malignancies, while preserving essential biological functions of Bcl-XI in other cells.

To conclude, our study is the first to reveal a difference in the cellular activity of the BH4 domain of Bcl-2 and Bcl-XI toward IP₃R regulation because of a single residue difference between both domains.

Materials and Methods

Peptides. All synthetic peptides were obtained from Thermo Electron (Osterode, Germany). Biotinylated peptides were obtained from Lifetein (South Plainfield, NJ, USA). Table 1 provides an overview of the different peptides used in this study and their primary sequence.

Plasmid vector constructs. The pGEX-6p2 construct (Amersham Biosciences, GE Healthcare, Diegem, Belgium) encoding a.a. 923–1581 of mouse IP₃R1 Domain 3 was obtained as previously described.²⁸ pcDNA3.1 (-) mouse IP₃R2 and rat IP₃R3 were used as templates for the construction of pGEX-6p2 vectors encoding the corresponding regions of IP₃R2 (a.a. 913–1562) and IP₃R3 (a.a. 910–1427). Their respective coding regions were amplified by PCR using the following primers: IP₃R2 forward (5'-GCGGCGGGATCCAATGTCTGAGGACCATCCACGG-3'); IP₃R2 reverse (5'-GCGGCGGAATTCCTAGAGCGTGTGACCTGGCTG-3'); IP₃R3 forward (5'-GCGGCGGGATCCAACGTGCGGAGGTCATCCAGGG-3'); IP₃R3 reverse (5'-GCGGCGGAATTCACAGAGCGCTCATGTGGGCATC-3'). PCR products were purified, digested with *Bam*HI and *Eco*RI (restrictions sites are underlined above) and ligated into *Bam*HI–*Eco*RI-treated pGEX-6p2 vector.

3xFLAG-Bcl-2 and -Bcl-XI were generated by subcloning their respective full-length cDNAs into p3xFLAG-myc-CMV-24 vector (Sigma-Aldrich, Munich, Germany) at *Hind*III/*Bgl*II sites. The 3xFLAG-Bcl-2 K/D mutant was generated by PCR site-directed mutagenesis introducing GAT (D) to replace AAG (K) in wild-type Bcl-2-donor DNA. The following primers were used: 3F-Bcl-2 K/D forward (5'-GATAACCGGGAGATAGTGATGGATTACATCCATTATAAGCTGTCCG-3'); 3F-Bcl-2 K/D reverse (5'-CGACAGCTTATAATGGATGTAATCCATCACTATCTCCCGTTATC-3').

The pSFFV-Neo and pSFFV-Neo-Bcl-2 vectors were kindly provided by Professor Clark W Distelhorst. The pSFFV-Neo-Bcl-2 K/D vector was also obtained by PCR site-directed mutagenesis. To introduce the desired point mutations, we designed and used the following primers: Neo-Bcl-2 K/D forward (5'-GACAACCGGGAGATAGTGATGGACTACATCCATTATAAGCTGTCCG-3'); Neo-Bcl-2 K/D reverse (5'-CGACAGCTTATAATGGATGTAATCCATCACTATCTCCCGTTGTC-3'). All constructs were verified by sequencing (Agowa AG, Berlin, Germany).

Figure 7 Mutating Lys17 into Asp in full-length Bcl-2 largely prevents the ability of Bcl-2 to bind to the IP₃R, inhibit IP₃R-mediated Ca²⁺ release and protect against STS-induced apoptosis in COS-1 cells. (a) Lysates from 3xFLAG-Bcl-2- and 3xFLAG-Bcl-2 K/D-overexpressing COS-1 cells were used in GST pull-down assays using purified GST-Dom3. A representative western blot using anti-FLAG antibodies is shown. (b) Immunoreactive bands of at least five independent experiments were quantified using ImageJ software. Values represent normalized values relative to their binding to GST. (c–e) COS-1 cells were co-transfected with mCherry plasmids and threefold excess of either empty vector (c), 3xFLAG-Bcl-2 plasmid (d) or 3xFLAG-Bcl-2 K/D plasmid (e). Only cells expressing the mCherry plasmid were monitored as F340/F380. Fura-2 signals were calibrated to obtain [Ca²⁺] (nM). Representative Ca²⁺ traces obtained from 10 Fura-2-loaded COS-1 cells in response to ATP (1 μM) are shown. (f) Quantitative analysis of the amplitude of the ATP-induced Ca²⁺ signals in mCherry-expressing COS-1 cells transfected with either empty vector, 3xFLAG-Bcl-2 plasmid or 3xFLAG-Bcl-2 K/D plasmid obtained from six independent experiments (mean ± S.E.M.). *Both 3xFLAG-Bcl-2 and 3xFLAG-Bcl-2 K/D significantly reduce the peak [Ca²⁺] in response to ATP. [§]3xFLAG-Bcl-2 K/D is significantly different from 3xFLAG-Bcl-2. (g) Quantitative analysis of the area under the curve of the TG-induced Ca²⁺ signal in these cells. (h) Western-blot analysis using anti-PARP antibodies for monitoring PARP cleavage upon STS treatment (1 μM for 6 h) in 3xFLAG-vector, 3xFLAG-Bcl-2 and 3xFLAG-Bcl-2 K/D-expressing COS-1 cells. GAPDH was used as a loading control. (i) Quantification of the immunoreactive bands of the ratio of the cleaved over the full-length PARP in the different transfected COS-1 cell populations from three independent experiments. The ratio of cleaved over full-length PARP obtained for control cells were set at 100% and the other ratios were normalized to this value. Both 3xFLAG-Bcl-2 and 3xFLAG-Bcl-2 K/D significantly (*) prevent STS-induced apoptosis compared with the empty-vector control, but 3xFLAG-Bcl-2 K/D is significantly (§) less potent than 3xFLAG-Bcl-2. Statistically significant differences are indicated as in Figure 5. We wish to remark that the results obtained with 3xFLAG-Bcl-2 K/D were borderline significantly (*) different from the empty-vector control (P = 0.051)

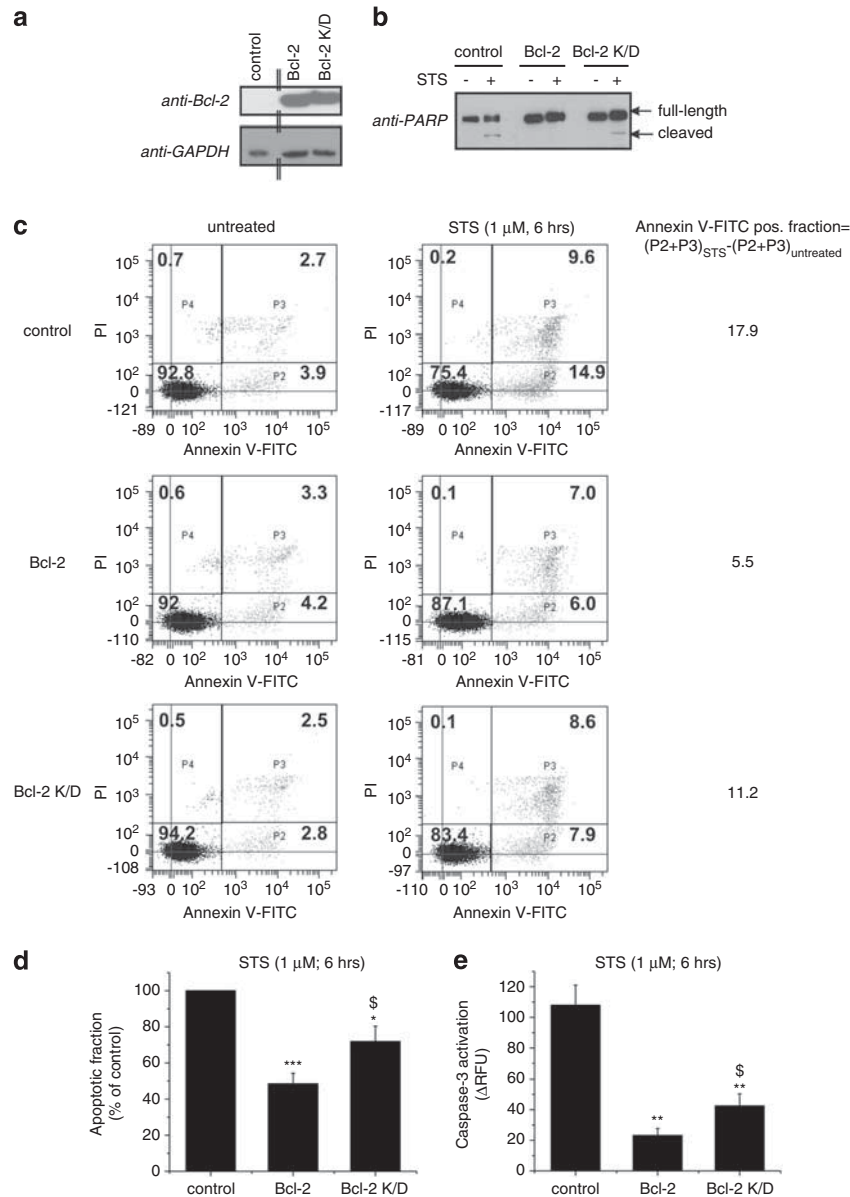


Figure 8 Bcl-2 K/D is less effective than Bcl-2 in protecting against STS-induced apoptosis in stable WEHI7.2 cell lines. **(a)** Stable WEHI7.2 cell lines expressing Bcl-2 or Bcl-2 K/D were created. The expression levels of Bcl-2 and Bcl-2 K/D were examined by western-blotting analysis using an anti-Bcl-2 antibody. Control WEHI7.2 cells display very low endogenous Bcl-2 levels. **(b)** The cleavage of poly(ADP-ribose)-polymerase (PARP) in control WEHI7.2 cells, WEHI7.2 cells expressing Bcl-2 and WEHI7.2 cells expressing Bcl-2 K/D was monitored by western-blotting analysis using an anti-PARP antibody. **(c)** FACS analysis of untreated and STS-treated PI/Annexin V-FITC-stained control, Bcl-2-overexpressing and Bcl-2 K/D-overexpressing WEHI7.2 cell lines (10 000 cells per analysis). The apoptotic population was identified as the AnnexinV-FITC-positive fraction (P2 + P3). The STS-induced apoptotic population was determined by the difference between the Annexin V-FITC-positive fraction of STS-treated cells and the untreated cells: $(P2 + P3)_{STS} - (P2 + P3)_{untreated}$. **(d)** Quantitative analysis from five independent experiments of the STS-induced apoptotic cell population, normalized to the values obtained for the control WEHI7.2 cells (% of control). **(e)** Fluorimetric analysis from three independent experiments of the caspase-3 activity in untreated and STS-treated control, Bcl-2-overexpressing and Bcl-2 K/D overexpressing WEHI7.2 cells using a plate-reader assay. The difference in relative fluorescence units between STS-treated and untreated cells was calculated and plotted. In all these experiments, both Bcl-2 and Bcl-2 K/D significantly (*) protected against STS-induced apoptosis, but Bcl-2 K/D was significantly (\$) less potent than Bcl-2. Statistically significant differences are indicated as in Figure 5

Cell culture and transfections. MEF cells were cultured at 37°C in a 9% CO₂ incubator in DMEM/Ham's F12 medium (1 : 1; Invitrogen, Merelbeke, Belgium) supplemented with 10% fetal calf serum (Sigma-Aldrich), 3.8 mM L-glutamine (Glutamax, Invitrogen), 85 IU/ml penicillin and 85 μ g/ml streptomycin (Invitrogen). C6 glioma cells were cultured in DMEM/Ham's F12 medium (1 : 1), containing 10% fetal calf serum, 100 IU/ml penicillin, 100 μ g/ml streptomycin, 2.5 μ g/ml fungizone and 2 mM L-glutamine at 37°C, 5% CO₂. COS-1 cells were seeded at a density of 15 000 cells/cm² and cultured in DMEM supplemented with 10% fetal bovine serum

(Sigma-Aldrich) at 37°C, 10% CO₂. At 2 days after plating, COS-1 cells were transiently transfected with the empty p3xFLAG-Myc-CMV-24 vector (Sigma-Aldrich) or containing the cDNA of Bcl-2 or of the Bcl-2 K/D mutant. The transfection procedure was performed using JetPRIME transfection reagent (Polyplus Transfections, New York, NY, USA) and following the manufacturer's recommendations. For Ca²⁺ imaging experiments, COS-1 cells were also co-transfected with a pcDNA 3.1-mCherry vector (Invitrogen) using a DNA ratio of 1 : 2 between pcDNA 3.1-mCherry and p3xFLAG-Myc-CMV-24 vectors.

Table 1 Overview of the sequence of different peptides used in this study

| Peptide name | Peptide sequence |
|-------------------------|-----------------------------------|
| BH4-Bcl-2 | RTGYDNR EIVMKYIHYKLSQRGYEW |
| BH4-Bcl-XI | MSQSNREL VVDFLSYKLSQKGYSW |
| BH4-Bcl-2SCR | WYEKQRSLHGIMYYVIEDRNTKGYR |
| BH4-Bcl-2BIND | RTGYANAEIVMKYIAEKLSAAGKEW |
| BH4-Bcl-2 K/D | RTGYDNR EIVMKYIHYKLSQRGYEW |
| BH4-Bcl-XI D/K | MSQSNREL VVDFLSYKLSQKGYSW |
| IDP | NVYTEIKCNLLPLDDIVRV |
| Biotin-BH4-Bcl-2 | Biotin-RTGYDNR EIVMKYIHYKLSQRGYEW |
| Biotin-BH4-Bcl-XI | Biotin-MSQSNREL VVDFLSYKLSQKGYSW |
| Biotin-BH4-Bcl-2SCR | Biotin-WYEKQRSLHGIMYYVIEDRNTKGYR |
| Biotin-BH4-Bcl-XISCR | Biotin-WYSKQRSLSGLVVMYVLEDKNSQFS |
| Biotin-BH4-Bcl-2BIND | Biotin-RTGYANAEIVMKYIAEKLSAAGKEW |
| Biotin-BH4-Bcl-2BINDSCR | Biotin-WKEKAASLAGIMEYVIEAANTKGYR |
| Biotin-BH4-Bcl-2 K/D | Biotin-RTGYDNR EIVMKYIHYKLSQRGYEW |
| Biotin-BH4-Bcl-XI D/K | Biotin-MSQSNREL VVKFLSYKLSQKGYSW |

WEHI7.2 murine cells were grown as described previously²⁸ and nucleofected with either pSFFV-Neo, pSFFV-Neo-Bcl-2 or pSFFV-Neo-Bcl-2 K/D vectors, using the Amaxa nucleofector and the dedicated Mouse T cell Nucleofector Kit according to the manufacturer's instructions (Amaxa-Lonza AG, Basel, Switzerland). Subsequently, resistant cells were stably selected with 1 mg/ml G418 (Invitrogen) as described in Chen *et al.*,²¹ but no clonal expansion was performed.

Western-blot analysis and antibodies. COS-1 and WEHI7.2 cells were lysed in a buffer containing 25 mM Hepes, pH 7.5, 1% Triton X-100, 10% glycerol, 0.3 M NaCl, 1.5 mM MgCl₂, 1 mM DTT, 2 mM EDTA, 2 mM EGTA and protease inhibitor cocktail tablets (Roche, Basel, Switzerland). The protein concentration of samples was determined by Bradford assay (Sigma-Aldrich) using bovine serum albumin (BSA) as standard. Proteins (10–20 µg) were separated by NuPAGE 4–12% Bis/Tris SDS-polyacrylamide gels using MES/SDS-running buffer (Invitrogen) and transferred onto a polyvinylidene fluoride (PVDF) membrane. After blocking with TBS containing 0.1% Tween and 5% non-fat dry milk powder, the membrane was incubated with the primary antibody overnight. Next, membranes were incubated for 1 h with a secondary horseradish peroxidase (HRP)-conjugated antibody (dilution 1 : 2000 in 0.1% Tween/TBS). Protein detection was performed with Pierce ECL Western Blotting Substrate (Thermo Fisher Scientific; p/a Perbio Science BVBA, Erembodegem, Belgium). Bands quantification was done with ImageJ software (rsbweb.nih.gov/ij/).

Primary antibodies used in this study are: mouse monoclonal ANTI-FLAG M2-Peroxidase (HRP) (Sigma-Aldrich), rabbit polyclonal anti-PARP-1 (Alexis-Enzo Life Sciences, Farmingdale, NY, USA), mouse monoclonal Anti-GAPDH clone GAPDH-71.1 (Sigma-Aldrich) and mouse monoclonal anti-Bcl-2 (C2) (Santa Cruz Biotechnology, Santa Cruz, CA, USA).

Unidirectional ⁴⁵Ca²⁺-flux assay. The 12-well clusters containing MEF cells were fixed on a thermostated plate at 30°C on a mechanical shaker. The culture medium was aspirated, and the cells were permeabilized by incubating them for 10 min in a solution containing 120 mM KCl, 30 mM imidazole-HCl (pH 6.8), 2 mM MgCl₂, 1 mM ATP, 1 mM EGTA and 20 µg/ml saponin. The non-mitochondrial Ca²⁺ stores were then loaded for 45 min in 120 mM KCl, 30 mM imidazole-HCl (pH 6.8), 5 mM MgCl₂, 5 mM ATP, 0.44 mM EGTA, 10 mM NaN₃ to prevent mitochondrial Ca²⁺ uptake, and 150 nM free ⁴⁵Ca²⁺ (28 µCi/ml). After reaching steady-state loading, cells were washed twice with 500 µl of efflux medium (120 mM KCl, 30 mM imidazole-HCl (pH 6.8), 1 mM EGTA) supplemented with 4 µM thapsigargin (Enzo Life Sciences, Farmingdale, NY, USA) to block SERCA (sarcolemmal-endoplasmic reticulum Ca²⁺ adenosine triphosphatase) Ca²⁺-uptake activity. Then, efflux medium was added and replaced every 2 min. IP₃ (3 µM) was added for 2 min after 10 min of efflux. At the end of the experiment, all ⁴⁵Ca²⁺ remaining in the stores were released by incubation with 1 ml of a 2% (w/v) SDS solution for 30 min. Ca²⁺ release was plotted as fractional loss (%/2 min) as a function of time as previously described.⁴⁶ The fractional loss represents the amount of Ca²⁺ leaving the store in a 2-min time period divided by the total store Ca²⁺ content at that time point. The effect of these BH4-domain peptides on IICR was tested by preincubating the peptides 4 min before exposing the stores to IP₃.

Electroporation loading. *In situ* electroporation of monolayer cell cultures was performed as described before,³² according to a procedure that was optimized for cell-death studies.³³ C6 cells were grown to near confluency on 13 mm diameter (apoptosis experiments) or 18 mm diameter (Fluo-3 Ca²⁺ imaging) glass coverslips. Cell-monolayer cultures were washed three times with Hanks' balanced salt solution buffered with Hepes (HBSS-Hepes) supplemented with D-glucose (0.81 mM MgSO₄, 0.95 mM CaCl₂, 137 mM NaCl, 0.18 mM Na₂HPO₄, 5.36 mM KCl, 0.44 mM KH₂PO₄, 5.55 mM D-glucose, 25 mM Hepes, pH 7.4) and subsequently three times with a low-conductivity electroporation buffer (4.02 mM KH₂PO₄, 10.8 mM K₂HPO₄, 1.0 mM MgCl₂, 300 mM sorbitol, 2.0 mM Hepes, pH 7.4). They were placed 400 µm underneath a two-wire Pt-Ir electrode on the microscopic stage and electroporated in the presence of a tiny amount of electroporation solution (10 µl). Electroporation was done with 50 kHz bipolar pulses applied as trains of 10 pulses of 2 ms duration each and repeated 15 times. The field strength was 100 V peak-to-peak applied over a 500 µm electrode separation distance. After electroporation, cells were thoroughly washed with HBSS-Hepes.

Fluo-3 Ca²⁺ imaging. C6 cells were seeded on 18 mm diameter glass coverslips and ester-loaded for 25 min with 5 µM Fluo-3-AM (Invitrogen) in HBSS-Hepes supplemented with 1 mM of probenecid (Sigma-Aldrich) and 0.01% pluronic F-127 (Invitrogen) at 37°C, followed by de-esterification over 15 min. Subsequently, cells were loaded with 100 µM Dextran Texas Red (DTR; Invitrogen) and 20 µM Bcl-2 peptides using the *in situ* electroporation technique as described above. For UV flash-photolysis experiments, 50 µM caged IP₃ (Invitrogen) was also included in the loading solution. Imaging was carried out using an inverted fluorescence microscope equipped with a × 40 oil-immersion objective and an intensified CCD camera (Extended Isis camera, Photonic Science, East Sussex, UK).

In the case of stimulation by ATP, cells were superfused for 1 min with HBSS-Hepes followed by 8 min with 1 µM of ATP (Sigma-Aldrich) in HBSS-Hepes, whereas for TG experiments, cells were superfused for 1 min with Ca²⁺-free HBSS-Hepes containing 1 mM EGTA followed by 7 min with 2.5 µM TG (Invitrogen) in the same buffer. For IP₃-photoliberation experiments, cells were, after 10 s, spot illuminated with 1-kHz pulsed UV light (349 nm UV laser Explorer, Spectra-Physics, Oxfordshire, UK) during 20 ms (20 pulses of 90 µJ energy measured at the entrance of the microscope epifluorescence tube). The UV flash was applied at five different places along the electroporated area per dish. Images (1/s) were generated with software written in Microsoft Visual C++ 6.0 (<http://msdn.microsoft.com/en-us/aa336402>). Fluorescence-intensity changes in different cells (at least 20) were analyzed with custom-developed FluoFrames software (generated by L Leybaert Lab.). For UV flash photolysis experiments, fluorescence-intensity changes in all cells in a predefined 3950 µm² region were analyzed. Ca²⁺-concentration, (Ca²⁺), changes were quantified as the area under the curve (AUC) of the separate Ca²⁺ traces. *N* is equal to the number of dishes.

Preparation of GST-fusion proteins. BL21(DE3) *Escherichia coli* cells were transformed with pGEX-6p2 constructs containing cDNAs of IP₃R1 domain 3 (GST-Dom3 IP₃R1: a.a. 923–1581), IP₃R2 domain-3 analog (GST-Dom3 IP₃R2: a.a. 913–1562), IP₃R3 domain-3 analog (GST-Dom3 IP₃R3: a.a. 910–1427) or with

the empty vector. The expressed proteins were purified as previously described.²⁸ All fusion proteins were affinity purified and dialyzed against standard phosphate-buffered saline (PBS) without added Ca^{2+} or Mg^{2+} (2.67 mM KCl, 1.47 mM KH_2PO_4 , 137.93 mM NaCl, 8.06 mM Na_2HPO_4 ; Invitrogen) using Slide-A-Lyzer with a cutoff of 3 kDa (Thermo Fisher Scientific, Pittsburg, PA, USA). After dialysis, the concentration of the purified GST-fusion proteins was determined using BCA Protein Assay Reagent (Thermo Fisher Scientific), and the quality and integrity were examined by SDS-PAGE and GelCode blue stain reagent (Thermo Fisher Scientific) before GST pull-downs or SPR analysis.

GST pull-downs. Equal amounts (30 μg) of the intact full-length GST-fusion proteins or parental GST (control) were incubated in Interaction Buffer (50 mM Tris-HCl, 300 mM NaCl, 1 mM EDTA, 1% NP-40, 0.5% sodium deoxycholate, 0.5% BSA and protease inhibitor cocktail, pH 7.0) with 30 μg of different BH4 domains (BH4-Bcl-2, BH4-Bcl-XI or a non-binding mutant (BH4-Bcl-2BIND)) and immobilized on glutathione-Sepharose 4B beads (GE Healthcare Europe GmbH, Munich, Germany) via rotation in a head-over-head rotator for 2 h at 4°C. The beads were washed four times with modified Interaction Buffer (150 mM NaCl instead of 300 mM NaCl, without BSA) and complexed GST-fusion proteins were eluted by incubating the beads with 40 μl LDS (Invitrogen) for 3 min at 95°C and collected after centrifuging at $500 \times g$ for 5 min. Eluates (10 μl) were subjected to western-blot analysis and the total protein content was visualized by GelCode blue staining of the gel.

For the pull-downs with full-length Bcl-2 proteins, 200 μg of cleared lysate from COS-1 cells transiently transfected with the 3xFLAG-Bcl-2 vector, 3xFLAG-Bcl-2-K/D or the empty vector were incubated with GST-tagged proteins using the same protocol as above. Eluates (10 μl) were subjected to western-blot and incubated with anti-FLAG HRP-conjugated antibody, diluted 1:4000 in 0.1% Tween/TBS.

SPR measurements. SPR experiments were performed as described before.⁴⁷ The binding of GST-Dom3 and parental GST (control) to the wild-type or mutated BH4 domain of Bcl-2 or Bcl-XI was analyzed by SPR at 25°C using a Biacore 2000 instrument (Uppsala, Sweden). Equal amounts (200 ng or 58.2 pmol) of > 80% pure biotinylated BH4 peptides were immobilized on four different flow cells of a streptavidin-coated sensor chip (BR-1000-32; Biacore, Uppsala, Sweden) using PBS supplemented with 0.005% P20 (Polysorbate-20) at pH 7.0. At least three independent sensor chips were used for the quantitative analysis.

Measurements with GST-fusion proteins as analyte were performed in PBS at a flow rate of 30 $\mu\text{l}/\text{min}$. Different concentrations of the analyte (injection volume 120 μl) were used in a random order to assess binding, expressed in terms of resonance units (RU). Bound peptide was removed by injection of 5 μl regeneration buffer (25 mM NaOH, 0.002% SDS) at 10 $\mu\text{l}/\text{min}$. Background signals were obtained from the reference flow cell, containing the BH4-scrambled peptide, and were subtracted to generate response curves using Biaevaluation 3.0 software (Biacore, <http://www.biacore.com>). In the analysis, only the association phase of the binding curve was taken into account. Data from two to three different sensorgrams for each condition were fitted by nonlinear regression analysis to a Hill–Langmuir binding isotherm using Origin 7.0 (OriginLab Corporation, Northampton, MA, USA) software.

Fura-2 Ca^{2+} imaging. At 2 days after co-transfection (mCherry + 3xFlag construct), COS-1 cells were loaded with Fura-2-AM (5 μM ; Biotium, Inc., Hayward, CA, USA) in modified Krebs buffer (135 mM NaCl, 5.9 mM KCl, 1.2 mM MgCl_2 , 11.6 mM Hepes, pH 7.3, 11.5 mM glucose and 1.5 mM Ca^{2+}) for 30 min, followed by de-esterification for 30 min. To buffer all free extracellular Ca^{2+} , 5 mM BAPTA (Invitrogen) was added before each measurement. ATP (1 μM) or TG (5 μM)-induced $[\text{Ca}^{2+}]$ rises were measured ratiometrically (excitation at 340 nm/380 nm, emission detection at 510 nm) using Zeiss Axio Observer Z1 Inverted Microscope equipped with a $\times 20$ air objective and an high-speed digital camera (Axiocam Hsm, Zeiss, Jena, Germany). Intracellular cytoplasmic Ca^{2+} concentrations ($[\text{Ca}^{2+}]_{\text{cyt}}$) were calculated from the equation: $[\text{Ca}^{2+}]_{\text{cyt}} (\text{nM}) = K_d \times Q \times (R - R_{\text{min}}) / (R_{\text{max}} - R)$, where K_d is the dissociation constant of Fura-2 for Ca^{2+} at room temperature (220 nM), Q is the fluorescence ratio of the emission intensity excited by 380 nm in the absence of Ca^{2+} to that in the presence of saturating Ca^{2+} , R is the fluorescence ratio, R_{min} and R_{max} are the minimal and maximal fluorescence ratios, respectively. The R_{min} was measured by perfusion with 50 mM EGTA in Ca^{2+} -free Krebs solution and R_{max} was obtained by perfusion with 5 μM ionomycin and 250 mM CaCl_2 . Only mCherry fluorescent (excitation 546 nm, emission 610 nm) and Fura-2 loaded cells were considered for data analysis. Per experiment, 10–15 cells were analyzed for a total of ~80 cells per transfection

condition on 3 different experimental days. Traces were normalized to baseline levels with Excel software (Microsoft Office) and for each experiment the average peak value ($\Delta[\text{Ca}^{2+}]_{\text{cyt}}$) was determined.

Apoptosis induction. For CytC-induced-apoptosis experiments, C6 cells were loaded by *in situ* electroporation in the presence of 100 μM DTR to identify the loaded zone, 20 μM of Bcl-2 peptides or 50 μM IP3RCYT peptide and 10 μM of CytC (Sigma). After electroporation, cells were kept in 200 μl culture medium for 25 min. For STS- and PAC-1-induced apoptosis experiments, cells were electroporated in the presence of 100 μM DTR and 20 μM Bcl-2 peptides. After electroporation, cells were kept in 200 μl culture medium containing 2 μM STS (Sigma-Aldrich) or 150 μM PAC-1 (Tocris Bioscience, Ellisville, MO, USA) for 6 h.

For STS-induced apoptosis, COS-1 cells transiently transfected with 3xFLAG-vectors and WEHI7.2 cells, and stably transfected with the various pSFFV-Neo vectors, were treated for 6 h with 1 μM STS (Sigma-Aldrich).

Detection of apoptosis by fluorescence microscopy. Glioma cells were stained first with 10 μM of the CaspACE FITC-VAD-FMK 'In situ Marker' (Promega Benelux, Leiden, The Netherlands) in HBSS-Hepes for 40 min at 37°C. After fixing the cells with 4% paraformaldehyde (PFA) for 25 min at room temperature, nuclei were additionally stained for 5 min with 1 $\mu\text{g}/\text{ml}$ DAPI (Sigma) in PBS supplemented with Ca^{2+} and Mg^{2+} (PBSD+). Cells were mounted with Vectashield fluorescent mounting medium (VWR International, Leuven, Belgium) on glass slides.

Five images (in each culture) were taken in the electroporated area using a Nikon TE300 epifluorescence microscope equipped with a $\times 10$ objective (Plan APO, NA 0.45; Nikon) and a Nikon DS-5M camera (Nikon, Brussels, Belgium). The number of caspase-positive cells and DNA-fragmented nuclei were counted in each image and expressed relative to the number of nuclei present and stated as the AI. Small groups of apoptotic bodies were counted as remnants of a single apoptotic cell. Analyses were carried out blinded, making use of custom-developed counting software. For the STS- and PAC-1-treated cultures, five additional images were taken outside the electroporated area. The AI in the electroporated area was expressed relative to the AI outside the area.

FACS analysis and microplate-based apoptosis assay. WEHI7.2 cells were pelleted by centrifugation and incubated with Annexin-V-FITC (Becton Dickinson, USA) and PI (Invitrogen). Single-cell suspensions were analyzed by FACScanto (Becton Dickinson, Franklin Lakes, NJ, USA). Cell death by apoptosis and secondary necrosis was scored by quantifying the population of Annexin-V-FITC-positive cells and Annexin-V-FITC/PI-positive cells. Flow-cytometric data were plotted and analyzed using BD FACSDiva Software (Becton Dickinson). Results were normalized as percentage decrease over control conditions.

Caspase-3 activity of STS-treated-WEHI7.2 cells was measured according to the protocol of the commercially available NucView 488 Caspase-3 Kit for live Cells (Biotium). Cells were transferred to a 96-well plate at a density of 400 000 cells/well and fluorescence was monitored using a FlexStation 3 microplate reader (Molecular Devices, Sunnyvale, CA, USA). The fluorescence intensity units collected from treated cells were normalized to untreated controls and plotted as changes in relative fluorescence units (ΔRFU).

Data and statistical analysis. Data are expressed as mean \pm S.E.M., unless a typical experiment is shown (mean \pm S.D.). Statistically significant differences were considered at $P < 0.05$ (single symbols), $P < 0.01$ (double symbols) and $P < 0.001$ (triple symbols) after using a two-tailed paired Student's *t*-test (Excel Microsoft Office) or one-way ANOVA and a Bonferroni post-test using Origin 7.0.

Conflict of interest

The authors declare no conflict of interest.

Acknowledgements. We thank Marina Crabbe, Anja Florizoone and Kirsten Welkenhuyzen for excellent technical help. We thank Dr. Ylva Ivarsson for SPR training. We greatly appreciated the help of Dr. K Mikoshiba (Lab. for Developmental Neurobiology, Brain Science Institute, RIKEN, Japan), Dr. D Boehning (Department of Neuroscience and Cell Biology, University of Texas, Medical Branch, Texas, USA) and Dr. P Zimmermann (Dept. of Human Genetics,

KU Leuven), respectively, for providing the IP₃R2-expression plasmid, IP3RCYT peptide and the use of the BIAcore 2000. This work was supported by the Research Foundation-Flanders (FWO) Grant nos. G.0604.07N to HDS, G.0788.11N to GB and MDM and G.0134.09N to LL, by the Research Council of the KU Leuven via the Concerted Actions program (GOA/09/012) and via an OT START (STRT1/10/044), and by the Interuniversity Attraction Poles Program (Belgian Science Policy; P6/28 to HDS, JBP and LM and P6/31 to LL), and by National Institutes of Health RO1 CA085804 (to CWD). GM and ED were supported by a PhD fellowship from Research Foundation-Flanders (FWO). HA was supported by a postdoctoral fellowship from the Research Foundation-Flanders (FWO).

1. Chipuk JE, Moldoveanu T, Liambi F, Parsons MJ, Green DR. The BCL-2 family reunion. *Mol Cell* 2010; **37**: 299–310.
2. Brunelle JK, Letai A. Control of mitochondrial apoptosis by the Bcl-2 family. *J Cell Sci* 2009; **122**: 437–441.
3. Chipuk JE, Green DR. How do BCL-2 proteins induce mitochondrial outer membrane permeabilization? *Trends Cell Biol* 2008; **18**: 157–164.
4. Bertsch U, Deschmeier C, Fanick W, Girkontaite I, Hillemeier K, Johnen H *et al*. The second messenger binding site of inositol 1,4,5-trisphosphate 3-kinase is centered in the catalytic domain and related to the inositol trisphosphate receptor site. *J Biol Chem* 2000; **275**: 1557–1564.
5. Hunter JJ, Bond BL, Parslow TG. Functional dissection of the human Bcl2 protein: sequence requirements for inhibition of apoptosis. *Mol Cell Biol* 1996; **16**: 877–883.
6. Huang DC, Adams JM, Cory S. The conserved N-terminal BH4 domain of Bcl-2 homologues is essential for inhibition of apoptosis and interaction with CED-4. *EMBO J* 1998; **17**: 1029–1039.
7. Oakes SA, Lin SS, Bassik MC. The control of endoplasmic reticulum-initiated apoptosis by the BCL-2 family of proteins. *Curr Mol Med* 2006; **6**: 99–109.
8. Oakes SA, Opferman JT, Pozzan T, Korsmeyer SJ, Scorrano L. Regulation of endoplasmic reticulum Ca²⁺ dynamics by proapoptotic BCL-2 family members. *Biochem Pharmacol* 2003; **66**: 1335–1340.
9. Scorrano L, Oakes SA, Opferman JT, Cheng EH, Sorcinelli MD, Pozzan T *et al*. BAX and BAK regulation of endoplasmic reticulum Ca²⁺: a control point for apoptosis. *Science* 2003; **300**: 135–139.
10. Rong Y, Distelhorst CW. Bcl-2 protein family members: versatile regulators of calcium signaling in cell survival and apoptosis. *Annu Rev Physiol* 2008; **70**: 73–91.
11. Rizzuto R, Marchi S, Bonora M, Aguiari P, Bononi A, De Stefani D *et al*. Ca²⁺ transfer from the ER to mitochondria: when, how and why. *Biochim Biophys Acta* 2009; **1787**: 1342–1351.
12. Joseph SK, Hajnoczky G. IP₃ receptors in cell survival and apoptosis: Ca²⁺ release and beyond. *Apoptosis* 2007; **12**: 951–968.
13. Pinton P, Giorgi C, Siviero R, Zecchini E, Rizzuto R. Calcium and apoptosis: ER-mitochondria Ca²⁺ transfer in the control of apoptosis. *Oncogene* 2008; **27**: 6407–6418.
14. Hayashi T, Rizzuto R, Hajnoczky G, Su TP. MAM: more than just a housekeeper. *Trends Cell Biol* 2009; **19**: 81–88.
15. Spat A, Szanda G, Csordas G, Hajnoczky G. High- and low-calcium-dependent mechanisms of mitochondrial calcium signalling. *Cell Calcium* 2008; **44**: 51–63.
16. Decuyper JP, Monaco G, Missiaen L, De Smedt H, Parys JB, Bultynck G. IP₃ receptors, mitochondria, and Ca signaling: implications for aging. *J Aging Res* 2011; **2011**: 920178.
17. Bathori G, Csordas G, Garcia-Perez C, Davies E, Hajnoczky G. Ca²⁺-dependent control of the permeability properties of the mitochondrial outer membrane and voltage-dependent anion-selective channel (VDAC). *J Biol Chem* 2006; **281**: 17347–17358.
18. Csordas G, Renken C, Varnai P, Walter L, Weaver D, Buttle KF *et al*. Structural and functional features and significance of the physical linkage between ER and mitochondria. *J Cell Biol* 2006; **174**: 915–921.
19. Jones RG, Bui T, White C, Madesh M, Krawczyk CM, Lindsten T *et al*. The proapoptotic factors Bax and Bak regulate T cell proliferation through control of endoplasmic reticulum Ca²⁺ homeostasis. *Immunity* 2007; **27**: 268–280.
20. Oakes SA, Scorrano L, Opferman JT, Bassik MC, Nishino M, Pozzan T *et al*. Proapoptotic BAX and BAK regulate the type 1 inositol trisphosphate receptor and calcium leak from the endoplasmic reticulum. *Proc Natl Acad Sci USA* 2005; **102**: 105–110.
21. Chen R, Valencia I, Zhong F, McColl KS, Roderick HL, Bootman MD *et al*. Bcl-2 functionally interacts with inositol 1,4,5-trisphosphate receptors to regulate calcium release from the ER in response to inositol 1,4,5-trisphosphate. *J Cell Biol* 2004; **166**: 193–203.
22. Zhong F, Davis MC, McColl KS, Distelhorst CW. Bcl-2 differentially regulates Ca²⁺ signals according to the strength of T cell receptor activation. *J Cell Biol* 2006; **172**: 127–137.
23. White C, Li C, Yang J, Petrenko NB, Madesh M, Thompson CB *et al*. The endoplasmic reticulum gateway to apoptosis by Bcl-xL modulation of the InsP₃R. *Nat Cell Biol* 2005; **7**: 1021–1028.
24. Foskett JK, Yang Y, Cheung KH, Vais H. Bcl-xL regulation of InsP₃ receptor gating mediated by dual Ca²⁺ release channel BH3 domains. *Biophys J* 2009; **96** (3 Suppl 1): 391A.

25. Eckenrode EF, Yang J, Velmurugan GV, Foskett JK, White C. Apoptosis protection by Mcl-1 and Bcl-2 modulation of inositol 1,4,5-trisphosphate receptor-dependent Ca²⁺ signaling. *J Biol Chem* 2010; **285**: 13678–13684.
26. Li C, Wang X, Vais H, Thompson CB, Foskett JK, White C. Apoptosis regulation by Bcl-xL modulation of mammalian inositol 1,4,5-trisphosphate receptor channel isoform gating. *Proc Natl Acad Sci USA* 2007; **104**: 12565–12570.
27. Hanson CJ, Bootman MD, Distelhorst CW, Wojcikiewicz RJ, Roderick HL. Bcl-2 suppresses Ca²⁺ release through inositol 1,4,5-trisphosphate receptors and inhibits Ca²⁺ uptake by mitochondria without affecting ER calcium store content. *Cell Calcium* 2008; **44**: 324–338.
28. Rong YP, Aromolaran AS, Bultynck G, Zhong F, Li X, McColl K *et al*. Targeting Bcl-2-IP₃ receptor interaction to reverse Bcl-2's inhibition of apoptotic calcium signals. *Mol Cell* 2008; **31**: 255–265.
29. Rong YP, Bultynck G, Aromolaran AS, Zhong F, Parys JB, De Smedt H *et al*. The BH4 domain of Bcl-2 inhibits ER calcium release and apoptosis by binding the regulatory and coupling domain of the IP₃ receptor. *Proc Natl Acad Sci USA* 2009; **106**: 14397–14402.
30. Rong YP, Barr P, Yee VC, Distelhorst CW. Targeting Bcl-2 based on the interaction of its BH4 domain with the inositol 1,4,5-trisphosphate receptor. *Biochim Biophys Acta* 2009; **1793**: 971–978.
31. Li C, Fox CJ, Master SR, Bindokas VP, Chodosh LA, Thompson CB. Bcl-X(L) affects Ca²⁺ homeostasis by altering expression of inositol 1,4,5-trisphosphate receptors. *Proc Natl Acad Sci USA* 2002; **99**: 9830–9835.
32. De Vuyst E, De Bock M, Decrock E, Van Moorhem M, Naus C, Mabilde C *et al*. In situ bipolar electroporation for localized cell loading with reporter dyes and investigating gap junctional coupling. *Biophys J* 2008; **94**: 469–479.
33. Decrock E, De Vuyst E, Vinken M, Van Moorhem M, Vranckx K, Wang N *et al*. Connexin 43 hemichannels contribute to the propagation of apoptotic cell death in a rat C6 glioma cell model. *Cell Death Differ* 2009; **16**: 151–163.
34. Muchmore SW, Sattler M, Liang H, Meadows RP, Harlan JE, Yoon HS *et al*. X-ray and NMR structure of human Bcl-xL, an inhibitor of programmed cell death. *Nature* 1996; **381**: 335–341.
35. Lee LC, Hunter JJ, Mujeeb A, Turck C, Parslow TG. Evidence for alpha-helical conformation of an essential N-terminal region in the human Bcl2 protein. *J Biol Chem* 1996; **271**: 23284–23288.
36. Boehning D, Patterson RL, Sedaghat L, Glebova NO, Kurosaki T, Snyder SH. Cytochrome c binds to inositol (1,4,5) trisphosphate receptors, amplifying calcium-dependent apoptosis. *Nat Cell Biol* 2003; **5**: 1051–1061.
37. Boehning D, van Rossum DB, Patterson RL, Snyder SH. A peptide inhibitor of cytochrome c/inositol 1,4,5-trisphosphate receptor binding blocks intrinsic and extrinsic cell death pathways. *Proc Natl Acad Sci USA* 2005; **102**: 1466–1471.
38. Kruman I, Guo Q, Mattson MP. Calcium and reactive oxygen species mediate staurosporine-induced mitochondrial dysfunction and apoptosis in PC12 cells. *J Neurosci Res* 1998; **51**: 293–308.
39. Nutt LK, Chandra J, Pataer A, Fang B, Roth JA, Swisher SG *et al*. Bax-mediated Ca²⁺ mobilization promotes cytochrome c release during apoptosis. *J Biol Chem* 2002; **277**: 20301–20308.
40. Putt KS, Chen GW, Pearson JM, Sandhorst JS, Hoagland MS, Kwon JT *et al*. Small-molecule activation of procaspase-3 to caspase-3 as a personalized anticancer strategy. *Nat Chem Biol* 2006; **2**: 543–550.
41. Palmer AE, Jin C, Reed JC, Tsien RY. Bcl-2-mediated alterations in endoplasmic reticulum Ca²⁺ analyzed with an improved genetically encoded fluorescent sensor. *Proc Natl Acad Sci USA* 2004; **101**: 17404–17409.
42. Kaufmann T, Schlupf S, Sanz J, Neubert K, Stein R, Borner C. Characterization of the signal that directs Bcl-xL, but not Bcl-2, to the mitochondrial outer membrane. *J Cell Biol* 2003; **160**: 53–64.
43. Shimizu S, Konishi A, Kodama T, Tsujimoto Y. BH4 domain of antiapoptotic Bcl-2 family members closes voltage-dependent anion channel and inhibits apoptotic mitochondrial changes and cell death. *Proc Natl Acad Sci USA* 2000; **97**: 3100–3105.
44. Cory S, Huang DC, Adams JM. The Bcl-2 family: roles in cell survival and oncogenesis. *Oncogene* 2003; **22**: 8590–8607.
45. Zhong F, Harr MW, Bultynck G, Monaco G, Parys JB, De Smedt H *et al*. Induction of Ca²⁺-driven apoptosis in chronic lymphocytic leukemia cells by peptide-mediated disruption of Bcl-2-IP₃ receptor interaction. *Blood* 2011; **117**: 2924–2934.
46. Decuyper JP, Monaco G, Kiviluoto S, Oh-hora M, Luyten T, De Smedt H *et al*. STIM1, but not STIM2, is required for proper agonist-induced Ca²⁺ signaling. *Cell Calcium* 2010; **48**: 161–167.
47. Ponsaerts R, De Vuyst E, Retamal M, D'Hondt C, Vermeire D, Wang N *et al*. Intramolecular loop/tail interactions are essential for connexin 43-hemichannel activity. *FASEB J* 2010; **24**: 4378–4395.



This work is licensed under the Creative Commons Attribution-NonCommercial-Share Alike 3.0 Unported License. To view a copy of this license, visit <http://creativecommons.org/licenses/by-nc-sa/3.0/>

Supplementary Information accompanies the paper on Cell Death and Differentiation website (<http://www.nature.com/cdd>)